

Dynamic upscaling of decomposition kinetics for carbon cycling models

Arjun Chakrawal^{1,2}, Anke M. Herrmann³, Johannes Koestel³, Jerker Jarsjö^{1,2}, Naoise Nunan⁴, Thomas Kätterer⁵, and Stefano Manzoni^{1,2}

¹Department of Physical Geography, Stockholm University, Svante Arrhenius väg 8C, Frescati, SE-106 91 Stockholm, Sweden

²Bolin Centre for Climate Research, Stockholm University, Stockholm, Sweden

³Department of Soil & Environment, Swedish University of Agricultural Sciences, P. O. Box 7014, 75007 Uppsala, Sweden

⁴Institute of Ecology and Environmental Sciences - Paris, Sorbonne Université-CNRS-IRD-INRA-P7-UPEC, 4 place Jussieu, 75005 Paris, France

⁵Department of Ecology, Swedish University of Agricultural Sciences, P. O. Box 7044, 75007 Uppsala, Sweden

Correspondence: Arjun Chakrawal (arjun.chakrawal@natgeo.su.se)

Abstract. The distribution of organic substrates and microorganisms in soils is spatially heterogeneous at the micro-scale. Most soil carbon cycling models do not account for this micro-scale heterogeneity, which may affect predictions of carbon (C) fluxes and stocks. In this study, we hypothesize that the mean respiration rate \bar{R} at the soil-core scale (i) is affected by the micro-scale spatial heterogeneity of substrate and microorganisms and (ii) depends upon the degree of this heterogeneity.

5 To assess theoretically the effect of spatial heterogeneities on \bar{R} , we contrast heterogeneous conditions with isolated patches of substrate and microorganisms versus spatially homogeneous conditions equivalent to those assumed in most soil C models. Moreover, we distinguish between biophysical heterogeneity, defined as the non-uniform spatial distribution of substrate and microorganisms, and full heterogeneity, defined as the non-uniform spatial distribution of substrate quality (or accessibility) in addition to biophysical heterogeneity.

10 Four common formulations for decomposition kinetics (linear, multiplicative, Michaelis-Menten, and inverse Michaelis-Menten) are considered in a coupled substrate-microbial biomass model valid at the micro-scale. We start with a 2D domain characterized by a heterogeneous substrate distribution and numerically simulate organic matter dynamics at each cell in the domain. To interpret the mean behavior of this spatially-explicit system, we propose an analytical scale transition approach in which micro-scale heterogeneities affect \bar{R} through the second order spatial moments (spatial variances and covariances).

15 The model assuming homogeneous conditions was not able to capture the mean behavior of the heterogeneous system because the second order moments cause \bar{R} to be higher or lower than in the homogeneous system, depending on the sign of these moments. This effect of spatial heterogeneities appears in the up-scaled nonlinear decomposition formulations, whereas the up-scaled linear decomposition model deviates from homogeneous conditions only when substrate quality is heterogeneous.

Thus, this study highlights the inadequacy of applying at the macro-scale the same decomposition formulations valid at the micro-scale, and proposes a scale transition approach as a way forward to capture micro-scale dynamics in core-scale models.

1 Introduction

Soil organic substrates and microorganisms are heterogeneously distributed in the soil medium (Nunan et al., 2002; Peth et al., 2014; Raynaud and Nunan, 2014; Rawlins et al., 2016). The importance of this heterogeneous distribution in soil organic matter (SOM) dynamics has been shown both experimentally and in modeling studies. Early experimental results show that the mineralization of SOM is affected by the non-uniform distribution of the substrates within macro and micro pores (Killham et al., 1993). The recognition that the spatial location of substrates and microorganisms constrains decomposition and thus C persistence is causing a paradigm shift from the previous emphasis on chemical composition of organic substrates to a focus on the biophysical environment in which decomposition occurs (Schmidt et al., 2011; Don et al., 2013; Schneckner et al., 2019). Soil pore structure is emerging as a fundamental property that integrates these biophysical constraints (Dungait et al., 2012; Falconer et al., 2015; Fraser et al., 2016). The biophysical and biochemical properties of the pore structure such as pore connectivity, tortuosity of water and air diffusion pathways, and adsorption/desorption, limit the access decomposers have to organic substrates. As a result, these micro-scale constraints create a spatially heterogeneous landscape with highly variable distributions of substrate and microbial C. In the following, we refer to this type of variability as micro-scale heterogeneity.

Despite the importance of micro-scale heterogeneities, most SOM decomposition models are based on reaction kinetics that are valid in well-mixed media, including C cycling schemes implemented in ecosystem and Earth system models. In well-mixed systems, the mean concentrations of substrate and microbial C, and the rates defined using these mean values are assumed to be representative of the system. Most existing SOM models embrace this assumption regardless of whether they are microbial implicit (i.e., based on first order kinetics) or microbial explicit (i.e., based on multiplicative and enzyme kinetics) (Manzoni and Porporato, 2009). This approach is often referred to as mean-field approximation and is meant to describe spatially averaged SOM dynamics at soil core- to plot-scales. There is an underlying, but untested, assumption that the kinetics that are valid under well mixed conditions at fine scales also hold at larger scales, where conditions are often far from well-mixed. For this assumption to hold, a spatially averaged C flux should be equal to the average flux when organic C is uniformly distributed throughout the system. This is not the case when C concentrations vary spatially and the kinetics are nonlinear (Chesson, 1998; Melbourne and Chesson, 2006; Morozov and Poggiale, 2012; Van Oijen et al., 2017). For example, even in the simple case of only two soil patches, the overall C fluxes follow more complex behaviors than within an individual homogeneous patch, requiring the use of kinetics that differ from those applied at the micro-scale (Manzoni et al., 2008).

The use of the same decomposition kinetics across a wide range of spatial scales is therefore questionable in systems that are spatially heterogeneous and regulated by nonlinear kinetics.

To understand at which scale a model developed for well-mixed conditions is expected to work, both the spatial scale at which heterogeneities become important and the scale at which homogeneity can be assumed must be identified. The average inter-cell distance in soil is in the order of 10 μm (Raynaud and Nunan, 2014) and the median length of spatial correlation of SOM varies between approximately 40 and 175 μm (Rawlins et al., 2016). Furthermore, it has been argued that the pore class with diameters between 30 and 150 μm is the most important for microbial activity (Kravchenko and Guber, 2017). This heterogeneity occurring at scales from ~ 10 to 200 μm , is generally neglected in C cycling models. Below the ~ 50 μm scale, diffusion time scales can be assumed to be faster than advection and reaction time scales (Watt et al., 2006). Thus, it can be argued that below ~ 50 μm the assumption of homogeneity is likely to hold, while it is no longer valid above this threshold (see Section 2.1.1 for details). If homogeneity cannot be assumed, how should decomposition kinetics be described in soil cores or at larger scales that include strong spatial heterogeneity?

Including micro-scale heterogeneities in the kinetics of SOM models is recognized as a much needed advancement in the field (Manzoni and Porporato, 2009; Sierra and Muller, 2015; Wieder et al., 2015), though only a few attempts have been made in this direction (e.g., Ebrahimi and Or (2016); Van Oijen et al. (2017)). In contrast, there are several examples of upscaling schemes for chemical reactions networks (Tang and Riley, 2013, 2017). The challenge is therefore to develop spatially up-scaled models that describe SOM decomposition at the macro-scale while taking into account the micro-scale heterogeneities. Mathematically, this upscaling problem is equivalent to spatial averaging of the mass balance equations based on the well-mixed assumption written at the micro-scale.

Three types of upscaling approaches are often used for dynamical systems such as those used to describe soil biogeochemical processes: (i) spatial averaging of numerically simulated C flux fields, (ii) definition of effective parameters to capture fine-scale heterogeneity, and (iii) scale transition theory or volume averaging of the equations at the micro-scale. Spatial averaging of simulated dynamics at the micro-scale is relatively common (Allison, 2012; Kaiser et al., 2014; Yan et al., 2016; Wang and Allison, 2019), but this approach does not lend itself to analytical solutions that would offer insights into the effects of heterogeneity on macroscopic properties. The effective parameter approach, more common in sub-surface hydrology (e.g. Dagan (1987)), has been used to relate the macroscopic decomposition rate to the characteristic parameters of micro-scale heterogeneity, but only in a minimal ‘lumped’ model (Manzoni et al., 2008). The estimated effective parameters tend to be specific to studied scenarios and difficult to generalize. Here, we focus mainly on the third method based on scale transition theory, because this approach provides a dynamic link between micro- and macro-scale using spatial moment approximations.

Using scale transition theory, it is possible to obtain an analytical, but approximate representation of dynamics at the macro-scale by accounting for the heterogeneity at micro-scale.

Scale transition theory is based on spatial averaging of the dynamical equations themselves (as opposed to averaging known fluxes as in point (i)). For example, this approach has been used to study predator-prey population dynamics at the patch and regional scales (Bergström et al., 2006; Englund and Leonardsson, 2008; Barraquand and Murrell, 2013). In these examples, the macroscopic (regional) population dynamics is controlled by the mean population densities of predator and prey, which in turn relate to the spatial statistics of population densities at the micro-scale (patch). Similar approaches are also used in hydrology to calculate average hydrologic fluxes when soil and micro-climatic conditions are spatially heterogeneous (Albertson and Montaldo, 2003; Fatichi et al., 2015), and in groundwater hydrology to derive transport equations at the Darcy- or field-scale (in this field the approach is called ‘volume averaging’ (Dentz et al., 2011)). We are aware of only one study using similar techniques to scale up C and N fluxes in soils from plot to regional scale (Van Oijen et al., 2017). Specifically, an empirical nonlinear function was used to link methane and nitrous oxide fluxes to soil moisture and temperature in each grid cell (corresponding to the micro-scale model) and the scale transition theory was applied to calculate the mean fluxes at the regional scale. Such an analytical expression linking fluxes to C pools at any time point is not always available. In most C cycle models, the fluxes are calculated by solving first the mass balance equations for the C pools (i.e., a system of differential equations). Therefore, to proceed, these differential equations at micro-scale must be scaled-up. This upscaling exercise is expected to yield a set of differential equations describing the mass balances of the spatially averaged C compartments, including kinetics for the macro-scale C fluxes that depend on the degree of micro-scale heterogeneity.

Here, using scale transition theory, we develop a general theoretical approach to link micro- and macro-scales in SOM decomposition models. Two types of micro-scale heterogeneity are identified and accounted for: biophysical and biochemical. Biophysical heterogeneity is caused by the non-uniform spatial distribution of substrate and microorganisms (i.e., heterogeneous distribution of the state variables), and biochemical heterogeneity is a result of spatial variations in substrate quality and thus turnover rates (i.e., heterogeneous distribution of the values of kinetic constants). With the proposed upscaling approach, we test the hypotheses that the rate of decomposition (i) is affected by the micro-scale spatial heterogeneity of substrate and microbial C and (ii) depends upon the degree of spatial heterogeneity. Scale transition theory is applied to four types of micro-scale decomposition kinetics commonly employed in C cycling models: conventional linear, multiplicative (M), Michaelis-Menten (MM), and inverse Michaelis-Menten (IMM). Considering these kinetic laws allows us to assess the consequences of neglecting spatial heterogeneities in the most common C cycling models. Our specific objectives are

1. To develop an analytical upscaling solution for a two pool C model

2. To quantify the impact of different spatial structures of substrate C_s , microbial biomass C_b and kinetic parameters k on the C dynamics
 3. To compare the results of a spatially-explicit heterogeneous model to the homogeneous equivalent as a function of the degree of heterogeneity
- 5 While the proposed upscaling approach is general, we apply it to scale up pore-scale processes to the scale of a small soil core or laboratory soil sample. These theoretical developments can be applied to SOM models employed to study respiration and microbial responses to perturbations at this relatively small spatial scale, or in models describing dynamics at a larger scale over relatively uniform spatial domains.

2 Methods

10 2.1 Theory

We distinguish between ‘micro-scale’ equations valid at the small scale where the well-mixed assumption holds, from ‘macro-scale’ equations valid at a larger scale of interest, which result from spatial averaging of the microscopic equations. While our derivations are general, in the presented model setup and results, we interpret ‘macro-scale’ as the scale of a small soil core. The goal of spatial upscaling is to derive the macro-scale soil C dynamics by spatial averaging of the micro-scale dynamics.

- 15 To obtain the macro-scale dynamics we employ two approaches: (i) a numerical approach based on grid-scale simulations followed by spatial averaging (upper panel Fig. 1) and (ii) an analytical approach based on scale transition theory (lower panel Fig. 1). The first is a computationally demanding approach and requires solving the micro-scale equations at each cell of the domain grid. Spatial averages and variances are thus calculated numerically over the domain at each time point in the simulation. With the analytical approach, the dynamic equations are first averaged and then solved directly for the mean state
- 20 variables. The obtained analytical expressions are used to interpret the results of the numerical simulations.

To proceed, the spatial average operator for our 2D domain is defined as,

$$\overline{\chi(t)} = \frac{\int \int \chi(x, y, t) dx dy}{\int \int dx dy} \approx \frac{1}{N_x N_y} \sum_{i=1}^{N_x} \sum_{j=1}^{N_y} \chi_{i,j}(t), \quad (1)$$

- where the double integral extends to the whole 2D domain, χ is a generic variable (C_s or C_b) or C flux, and N_x and N_y are the number of grid cells in the x and y direction. The second equality allows estimating χ using the simulated time series of
- 25 the variable of interest in each grid cell (denoted by $\chi_{i,j}$). In contrast to numerically solving the problem at each grid cell,

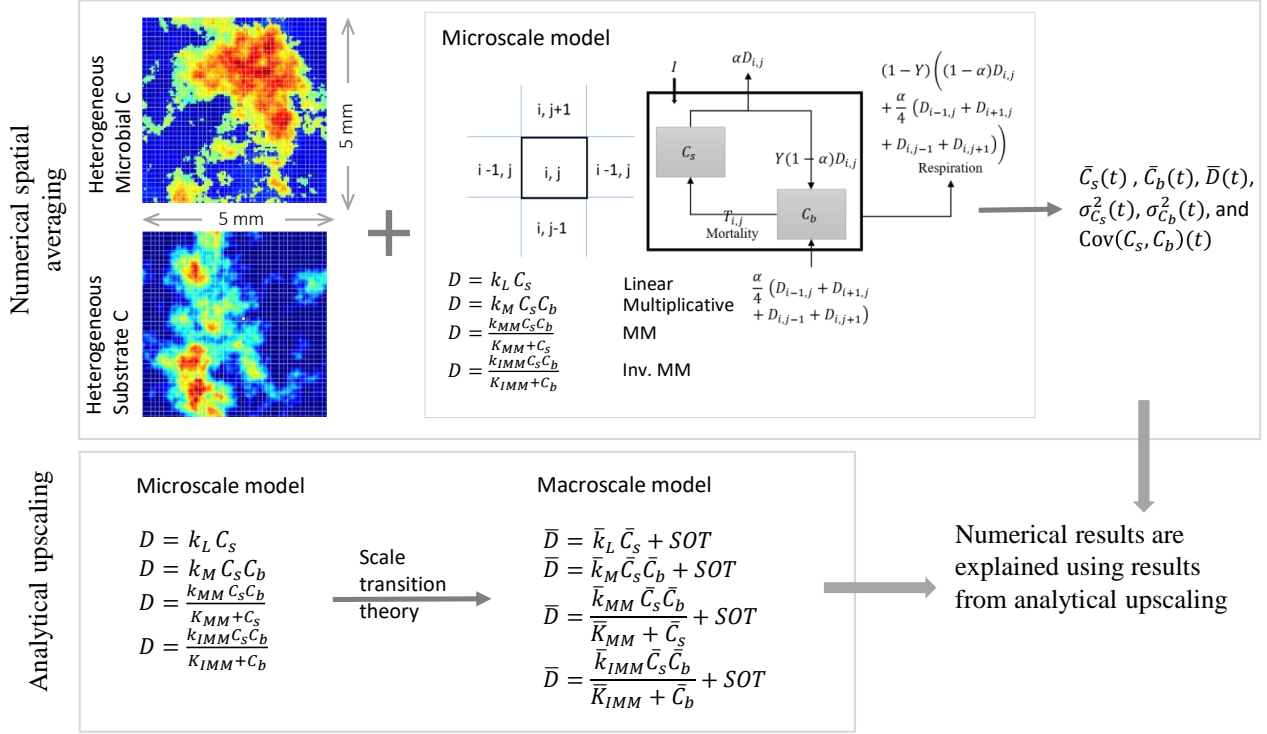


Figure 1. Schematic of two upscaling approaches used to study the C dynamics at the macro-scale. Numerical spatial averaging (top panel): the micro-scale model is applied at each grid cell of the heterogeneous domain; the mean C pools (substrate \bar{C}_s , and microbial biomass \bar{C}_b , where the overbar indicates spatial averaging), their mean fluxes, and second order spatial moments ($\sigma_{C_s}^2, \sigma_{C_b}^2, \overline{C'_s C'_b}$) are estimated by Eqs. (24)–(29) at each time step. This approach is referred to as ‘distributed model’. Analytical upscaling (bottom panel): the micro-scale decomposition flux is dynamically scaled up using scale transition theory, which provides the mean C fluxes as a function of mean C concentrations (mean-field approximation) and second order spatial moments representing the degree of heterogeneity. The deviations from the mean-field approximation are denoted as ‘second order terms’ (SOT) in the expressions for the mean decomposition fluxes (\bar{D} , where overbar represents mean quantities). The numerical results obtained from the distributed model are explained using the mathematical expression derived from analytical upscaling. This upscaling scheme is applied to four types of decomposition kinetics (linear, multiplicative, Michaelis-Menten, and inverse Michaelis-Menten), shown in the lower panel.

the analytical approach derives the dynamics of the macro-scale variables and fluxes using scale transition theory, discussed in Section 2.1.2.

2.1.1 Micro-scale model of soil carbon dynamics

The dynamics of soil organic C in a homogeneous medium are characterized by specific reaction kinetics that define organic C fluxes, and the number and arrangement of the soil C pools. For simplicity, we used a two pool model in which organic C is divided into (i) soil organic carbon substrate (C_s) and (ii) microbial biomass carbon (C_b) (Manzoni and Porporato, 2007; German et al., 2012). This simple structure was selected because it is at the core of most microbial explicit models (Zelenev et al., 2000; Schimel and Weintraub, 2003). It should be noted that conceptually we include in C_s only organic C that is available for de-polymerization and not stabilized; in other words we focus on decomposition time scales in the order of weeks to months. Modeling all the processes (and associated heterogeneity effects) leading to C stabilization is beyond our scope. The typical time scale of diffusive fluxes is given by $\tau_{diff} = x^2/D$ where x is the length scale of space discretization and D_{diff} is the diffusion coefficient (Hunt and Manzoni, 2015) and the typical time scale of reactive fluxes is given by the turnover time of the substrate; i.e., τ_{react} . The ratio of the two time scales defines the Damköhler number, $Da = \tau_{diff}/\tau_{react}$, which represents the relative importance of mass transport of the substrate via diffusion vs. reaction (Dentz et al., 2011). For a relevant substrate such as glucose, D_{diff} is the order of $10^{-11}\text{m}^2/\text{s}$ (Watt et al., 2006), the turnover time is in the order ~ 1 day and the length scale of the order of $\sim 50 \mu\text{m}$. With these values, $Da \ll 1$, which characterizes a reaction-limited system in well-mixed conditions. The result of this approximated calculation would not change with reaction time scales in the order of a few hours. Thus, the well-mixed assumption is valid at the scale of a pore of size $\sim 50 \mu\text{m}$; we refer to this model as the ‘micro-scale model’ (Fig. 1).

To include spatial fluxes across grid cells, we implemented a generic mass transfer mechanism. This mechanism is implemented by assuming that a fraction α of the decomposition rate D (i.e., αD) is transferred in equal amounts to the four neighboring grid cells. Hence, in each grid cell microorganisms receive additional C from neighboring grid cells at a rate $\frac{\alpha}{4} (D_{i-1,j} + D_{i+1,j} + D_{i,j-1} + D_{i,j+1})$. This choice is motivated by the observation that the products of de-polymerization are more soluble than stable organic matter and thus are more likely to be transported away from the site of decomposition. Thus, instead of modeling mobile carbon explicitly, we assumed that a fraction of the source of soluble C is transported to neighboring cells. This mass transfer mechanism can be interpreted as a consequence of various types of spatial redistribution,

including diffusion or bio-turbation. The micro-scale equations at one grid cell (control volume) take the following form,

$$\frac{dC_{s,i,j}}{dt} = I - D_{i,j} + T_{i,j}, \quad (2)$$

$$\frac{dC_{b,i,j}}{dt} = Y \left[(1 - \alpha)D_{i,j} + \frac{\alpha}{4} (D_{i-1,j} + D_{i+1,j} + D_{i,j-1} + D_{i,j+1}) \right] - T_{i,j}, \quad (3)$$

$$\frac{dCO_{2,i,j}}{dt} = (1 - Y) \left[(1 - \alpha)D_{i,j} + \frac{\alpha}{4} (D_{i-1,j} + D_{i+1,j} + D_{i,j-1} + D_{i,j+1}) \right], \quad (4)$$

5 where I is the rate of external input of organic C, D is the rate of decomposition, T is the microbial mortality, and Y is the microbial C use efficiency. The substrate C_s and microbial carbon C_b are the state variables of the micro-scale model, and their mass balances, Eqs. (2) and (3), describe their temporal evolution. If $\alpha = 0$, no mass transfer occurs and the model reduces to a simplified reactive system with two C pools, where grid cells are disconnected and thus independent. If $\alpha > 0$, mass transfer among the grid cells occurs. In this way, by changing the value of α , the effect of spatial redistribution on mean carbon
10 dynamics can be assessed. With $\alpha = 0$, the general mathematical description of the simplified micro-scale model is given by

$$\frac{dC_s}{dt} = I - D + T, \quad (5)$$

$$\frac{dC_b}{dt} = YD - T, \quad (6)$$

where for conciseness we removed the subscripts indicating grid cell positions. The rate of decomposition is described by four commonly used formulations: linear (Eq.7), multiplicative (M, Eq.8), Michaelis-Menten (MM, Eq.9), and inverse Michaelis-
15 Menten (IMM, Eq.10) (comparisons among these formulations can be found in Schimel and Weintraub (2003); Wutzler and Reichstein (2008); Manzoni and Porporato (2009)),

$$D = k_L C_s, \quad (7)$$

$$D = k_M C_s C_b, \quad (8)$$

$$D = k_{MM} \frac{C_s C_b}{K_{MM} + C_s} \quad (9)$$

$$20 \quad D = k_{IMM} \frac{C_s C_b}{K_{IMM} + C_b}, \quad (10)$$

where k_L , k_M , k_{MM} , and k_{IMM} are the decomposition rate constants for linear, multiplicative, MM, and IMM kinetics, respectively; and K_{MM} and K_{IMM} are the half saturation constants for the MM and IMM kinetics, respectively. Table 1 summarizes the functional forms of D and the steady state solutions of Eq. (5) and (6) for each case. Microbial mortality is

Table 1. Summary of the microscopic decomposition functions and steady state solutions

	Conventional (subscript L)	Multiplicative (subscript M)	Michaelis-Menten (subscript MM)	Inverse Michaelis-Menten (subscript IMM)
D	$k_L C_s$	$k_M C_s C_b$	$\frac{k_{MM} C_s C_b}{C_s + K_{MM}}$	$k_{IMM} \frac{C_s C_b}{K_{IMM} + C_b}$
T	$k_B C_b$	$k_B C_b$	$k_B C_b$	$k_B C_b$
Steady state C_s^*	$\frac{I}{(1-Y)k_L}$	$\frac{k_B}{Y k_M}$	$\frac{K_{MM} k_B}{Y k_{MM} - k_B}$	$\frac{K_{IMM} k_B (1-Y) + Y I}{Y (1-Y) k_{IMM}}$
Steady state C_b^*	$\frac{Y I}{(1-Y)k_B}$	$\frac{Y I}{(1-Y)k_B}$	$\frac{Y I}{(1-Y)k_B}$	$\frac{Y I}{(1-Y)k_B}$

assumed to follow first order kinetics ($T = k_B C_b$). We assume constant temperature and soil moisture conditions so that D is only a function of C_s and C_b . This assumption facilitates assessing the role of spatial heterogeneity of C substrates and microbial biomass in our idealized system. The analytical upscaling theory developed in the following section is based on the simplified micro-scale model given by Eqs. (5) and (6). For the mass-transfer model, only the numerical averaging method is used.

2.1.2 Spatial upscaling of soil carbon dynamics: scale transition theory

The scale transition theory is applied to study the C dynamics at micro- and macro-scale, and derive the changes in the structure of the equations describing the C pools and their fluxes at macro-scale. To upscale the micro-scale model, the spatial averaging operator given by Eq. (1) is applied to Eqs. (5) and (6), leading to the governing equations at the macro-scale,

$$10 \quad \frac{d\overline{C}_s}{dt} = \overline{I} - \overline{D} + \overline{T}, \quad (11)$$

$$\frac{d\overline{C}_b}{dt} = \overline{YD} - \overline{T}, \quad (12)$$

where the overbars denote the spatially averaged micro-scale quantities, so that \overline{D} and \overline{T} are the macro-scale rates of decomposition and microbial mortality. Since the order of averaging and differentiation can be exchanged, the right hand side of Eqs. (11) and (12) can be written as $\frac{d\overline{C}_s}{dt}$ and $\frac{d\overline{C}_b}{dt}$. Moreover, we assume that Y and I are spatially invariant, so that averaging does

not alter their values. The final mass balance equations for substrate and microbial C at macro-scale are thus given by

$$\frac{d\bar{C}_s}{dt} = I - \bar{D} + \bar{T}, \quad (13)$$

$$\frac{d\bar{C}_b}{dt} = Y\bar{D} - \bar{T}, \quad (14)$$

$$\bar{R} = \frac{d\bar{C}O_2}{dt} = (1 - Y)\bar{D}. \quad (15)$$

- 5 where \bar{R} is the mean respiration at macro-scale. In Eqs.(13)–(15), the macro-scale variables \bar{C}_s and \bar{C}_b can be obtained once the average fluxes \bar{D} and \bar{T} are known. The next step is therefore to express \bar{D} and \bar{T} as a function of macro-scale (\bar{C}_s, \bar{C}_b), and micro-scale state variables (C_s, C_b).

We can generalize the problem and consider a generic microscopic C flux (i.e. D or T) as a nonlinear (and smooth) function F of state variables C_s, C_b and a parameter vector \mathbf{k} ($[k_1, k_2, \dots, k_n]$), where n is the number of parameters. The spatial averages of C_s, C_b and k are denoted as \bar{C}_s, \bar{C}_b and $\bar{\mathbf{k}}$ ($[\bar{k}_1, \bar{k}_2, \dots, \bar{k}_n]$). Applying the averaging operator given by Eq. (1) to a multi-variate Taylor’s series expansion of $F(C_s, C_b, k)$ around the spatial average value of C_s, C_b and $\bar{\mathbf{k}}$ and truncating the series to second order gives the macroscopic C flux (detailed derivation is provided in Appendix A1),

$$\begin{aligned} \bar{F}(C_s, C_b, \mathbf{k}) = & F(\bar{C}_s, \bar{C}_b, \bar{\mathbf{k}}) + \frac{1}{2} \frac{\partial^2 F}{\partial C_s^2} \Big|_{\bar{C}_s, \bar{C}_b, \bar{\mathbf{k}}} \sigma_{C_s}^2 + \frac{1}{2} \frac{\partial^2 F}{\partial C_b^2} \Big|_{\bar{C}_s, \bar{C}_b, \bar{\mathbf{k}}} \sigma_{C_b}^2 + \sum_{i=1}^n \sum_{j=1}^n \frac{\partial^2 F}{\partial k_i \partial k_j} \Big|_{\bar{C}_s, \bar{C}_b, \bar{\mathbf{k}}} \overline{k'_i k'_j} + \\ & \frac{\partial^2 F}{\partial C_s \partial C_b} \Big|_{\bar{C}_s, \bar{C}_b, \bar{\mathbf{k}}} \overline{C'_s C'_b} + \sum_{i=1}^n \frac{\partial^2 F}{\partial k_i \partial C_s} \Big|_{\bar{C}_s, \bar{C}_b, \bar{\mathbf{k}}} \overline{k'_i C'_s} + \sum_{i=1}^n \frac{\partial^2 F}{\partial k_i \partial C_b} \Big|_{\bar{C}_s, \bar{C}_b, \bar{\mathbf{k}}} \overline{k'_i C'_b}, \end{aligned} \quad (16)$$

- 15 where prime symbols represent variations with respect to the spatial mean values, $\bar{F}(C_s, C_b, \mathbf{k})$ is the macroscopic C flux, $\sigma_{C_s}^2$ and $\sigma_{C_b}^2$ are the spatial variances of substrate and microbial C, respectively; $\overline{k'_i k'_j}$ is the spatial variance (if $i = j$) or spatial covariance (if $i \neq j$) between the micro-scale parameters; $\overline{C'_s C'_b}$, $\overline{k'_i C'_s}$ and $\overline{k'_i C'_b}$ are the spatial covariances between micro-scale substrate and microbial C, substrate and parameters, and microbial biomass and parameters, respectively.

In Eq. (16), the first term on the right hand side, $F(\bar{C}_s, \bar{C}_b, \bar{\mathbf{k}})$, represents the first order approximation of $\bar{F}(C_s, C_b, \mathbf{k})$, also known as ‘mean-field’ approximation (MFA). The MFAs for the chosen models are: $\bar{k}_M \bar{C}_s \bar{C}_b$ for multiplicative kinetics; $\bar{k}_{MM} \bar{C}_s \bar{C}_b / (\bar{K}_{MM} + \bar{C}_s)$ for Michaelis-Menten kinetics; $\bar{k}_{IMM} \bar{C}_s \bar{C}_b / (\bar{K}_{IMM} + \bar{C}_b)$ for inverse Michaelis-Menten kinetics. Most C cycling models neglect all the other terms in Eq. (16). The remaining six spatial variance and covariance terms in Eq. (16) are collectively referred to as ‘second order terms’ (SOT). Higher order terms can also be included by truncating the series beyond the SOT. We refer to all terms of order higher or equal to two as ‘high order terms’ (HOT). When the system is well-

mixed, all variances and covariance terms vanish, leaving only the MFA. Therefore, only considering the MFA is equivalent to assuming well-mixed conditions at the macro-scale (i.e., Eqs. (5) and (6) are equivalent to Eqs. (13) and (14)).

Equation (16) provides a proof that the ‘mean-field’ approximation is a specific case of the more general expression for a macroscopic C flux that also depends on spatial heterogeneity through the SOT. The MFA is valid only when either of the following two conditions are met. First, the micro-scale decomposition rate is assumed to follow first order kinetics with homogeneous k_L , because when F is a linear function of substrate and microbial C, the second order partial derivatives in Eq. (16) are zero. Second, C_s, C_b and kinetic parameters are spatially homogeneous, because in this case all the second order moments (spatial variances and covariances) are zero. However, if F is nonlinear, the second order partial derivatives are non-zero; similarly, if any type of micro-scale biophysical or biochemical heterogeneity is present, the SOT in Eq. (16) play a role in determining the macroscopic C dynamics.

Equation (16) illustrates the advantage of using scale transition theory as it provides an approximate analytical relation between the micro- and macro-scale quantities, which allows an immediate assessment of the role of both nonlinearities in the C flux formulations and spatial heterogeneities. Importantly, in some cases, Eq. (16) yields an exact (rather than approximated) equation for macro-scale quantities, as shown in the following section.

2.2 Effect of micro-scale heterogeneities on macro-scale dynamics

Depending upon the kinetics of the micro-scale decomposition model (Table 1), the macro-scale \bar{D} is expected to take different forms. Using different kinetic models, we now discuss some specific cases of micro-scale heterogeneities based on their biophysical or biochemical nature. Biophysical heterogeneity is characterized by the spatially heterogeneous distribution of substrate and microbial C, whereas biochemical heterogeneity is characterized by the spatially heterogeneous distribution of substrate quality and microbial properties, captured by the kinetic parameters. The inaccessibility of SOM can result in C persistence. Therefore, inaccessibility can be modelled (at least at a conceptual level) through low values of the kinetic rate constants, similar to biochemical properties. In the simple model used here, accessibility to substrates or chemical recalcitrance are not mechanistically distinguished, so variations in substrate ‘quality’ in the broadest sense can be interpreted as spatial heterogeneity in either chemical characteristics or accessibility at the micro-scale.

First, we focus on systems with only biophysical heterogeneity of substrate and microbial C. For the first order kinetics model, the rate of decomposition is given by $D = k_L C_s$, and using Eq. (16) and substituting $F = D = k_L C_s$, we obtain

$$\bar{D} = k_L \bar{C}_s. \tag{17}$$

In Eq. (17), \bar{D} has the same form as D , indicating that microbial-implicit first order kinetic models do not show any sensitivity to spatial heterogeneities because of the linearity of the decomposition function. For the multiplicative model, the rate of decomposition at the micro-scale is given by Eq. (8), and inserting Eq. (8) into Eq. (16) gives

$$\bar{D} = k_M \bar{C}_s \bar{C}_b + k_M \overline{C'_s C'_b}. \quad (18)$$

- 5 In Eq. (18), the biophysical heterogeneities play a role through the covariance term $\overline{C'_s C'_b}$. Note that Eq. (18) is an exact equation because all the spatial moments of order higher than two are zero. Thus, only the mean state variables and the spatial covariance are needed to fully characterize the macro-scale dynamics in this case. Furthermore, a positive spatial covariance (i.e. co-location of substrates and microorganisms) would increase the mean decomposition rate (\bar{D}), whereas a negative spatial covariance (i.e. spatial separation between substrates and microorganisms) would decrease it.
- 10 Similar to the multiplicative decomposition model, also in models based on MM and IMM kinetics, the rate of decomposition at the macro-scale depends on the covariance term $\overline{C'_s C'_b}$ and additional terms representing the spatial variances of the substrate and microbial C (Table 2). The spatial variance terms are always negative because variances are positive quantities and the partial derivatives multiplying the variances are negative in all decomposition functions that saturate at high substrate or microbial biomass concentration. In contrast, the spatial covariance term is positive or negative based on the sign of $\overline{C'_s C'_b}$.
- 15 Therefore, when using the MM or IMM kinetics, \bar{D} can be approximated by the MFA only if variance and covariance balance each other or are both negligible.

Second, we consider only biochemical heterogeneity. In this case, model parameters k vary spatially, but the initial values of the state variables C_s and C_b are assumed homogeneous. With linear decomposition, substituting $D = k_L C_s$ into Eq. (16) yields

$$20 \quad \bar{D} = \bar{k}_L \bar{C}_s + \overline{k'_L C'_s}. \quad (19)$$

Equation (19) shows that for a biochemical heterogeneous system, even the simplest linear model requires an additional covariance term to describe the governing equations at the macro-scale. This covariance term might change the linear microscopic model into a nonlinear macroscopic model. For the multiplicative model (Eq. (8)), Eq. (16) yields

$$\bar{D} = \bar{k}_M \bar{C}_s \bar{C}_b + \bar{C}_b \overline{k'_M C'_s} + \bar{C}_s \overline{k'_M C'_b}, \quad (20)$$

where $\overline{k'_M C'_s}$ and $\overline{k'_M C'_b}$ are respectively the spatial covariances between the state variables C_s , C_b and the rate constant parameter k_M . These two additional spatial covariance terms capture the effects of biochemical heterogeneity caused by the spatial variation in the rate constants of decomposition. Similar terms appear also when using the MM and IMM models.

5 Lastly, we consider a heterogeneous system with combined biophysical and biochemical heterogeneities, denoted as ‘fully heterogeneous’. Again, we use the multiplicative model to illustrate the relation between the dynamics at the micro- and macro-scale. Now, all the state variables and parameters in D at the micro-scale are spatially variable. For the multiplicative kinetics, k_M , C_s and C_b are spatially variable, so that inserting Eq. (8) into Eq. (16) gives

$$\overline{D} = \overline{k_M C_s C_b} + \overline{C_b k'_M C'_s} + \overline{C_s k'_M C'_b} + \overline{k_M C'_s C'_b}. \quad (21)$$

This generalized case includes all the spatial covariances between parameters and the state variables, thereby capturing biophysical and biochemical heterogeneities simultaneously. Moreover, Eqs. (20) and (21) are second order approximations, but an exact equation can be obtained by including a third order term $\overline{k'_M C'_s C'_b}$. A similar derivation is described for MM and IMM kinetics in the Appendix; however, an exact expression for the macro-scale decomposition rate for these two kinetics cannot be found and we only use the second order approximation. Table 2 provides a summary of the theoretical results for the discussed heterogeneous cases and for all four types of decomposition kinetics.

15 The same rationale used to derive Eq. (21) can be applied in systems where the C input rate I or the microbial C-use efficiency Y are not homogeneous as we assumed. This would cause additional second and higher order terms to appear in the macroscale equations, with consequences on the overall C balances.

Similar derivations can be done for the microbial mortality rate ($F = T$). The Taylor expansion of microbial mortality is simpler because we assume T to follow first order kinetics implying that all the second order terms are equal to zero. Therefore, 20 the mean field approximation is exact and spatial variance of this parameter has no effect on the macro-scale dynamics,

$$\overline{T} = k_B \overline{C_b}. \quad (22)$$

To illustrate how macro-scale decomposition kinetics are affected by spatial heterogeneity, we define a macro-scale specific growth rate (SGR) which is calculated by dividing the mean respiration rate by mean microbial C in the system.

$$SGR = \frac{\overline{R}}{\overline{C_b}} = (1 - Y) \frac{\overline{D}}{\overline{C_b}}. \quad (23)$$

Table 2. Summary of macro-scale equations for the decomposition rate (\bar{D})

	Biophysical heterogeneity	Biochemical heterogeneity	Full-heterogeneity
Linear	$k_L \bar{C}_s$	$\bar{k}_L \bar{C}_s + k'_L \bar{C}'_s$	$\bar{k}_L \bar{C}_s + k'_L \bar{C}'_s$
Multiplicative*	$k_M \bar{C}_s \bar{C}_b$ + $k_M \bar{C}'_s \bar{C}'_b$	$k_M \bar{C}_s \bar{C}_b$ + $\bar{C}_s \frac{k'_M \bar{C}'_b}{k'_M \bar{C}'_s}$ + $\bar{C}_b \frac{k'_M \bar{C}'_s}{k'_M \bar{C}'_b}$ + $k'_M \bar{C}'_s \bar{C}'_b$	$k_M \bar{C}_s \bar{C}_b$ + $\bar{C}_s \frac{k'_M \bar{C}'_b}{k'_M \bar{C}'_s}$ + $\bar{C}_b \frac{k'_M \bar{C}'_s}{k'_M \bar{C}'_b}$ + $k_M \bar{C}'_s \bar{C}'_b$ + $k'_M \bar{C}'_s \bar{C}'_b$
Michaelis-Menten	$\frac{k_{MM} \bar{C}_s \bar{C}_b}{K_{MM} + \bar{C}_s} +$ $\frac{1}{2} \left[\frac{-2k_{MM} K_{MM} \bar{C}_b}{(K_{MM} + \bar{C}_s)^3} \right] \sigma_{\bar{C}_s}^2 +$ $\left[\frac{k_{MM} K_{MM}}{(\bar{C}_s + K_{MM})^2} \right] \bar{C}'_s \bar{C}'_b$	Eq. (A8)	Eq. (A9)
Inverse Michaelis-Menten	$\frac{k_{IMM} \bar{C}_s \bar{C}_b}{K_{IMM} + \bar{C}_b} +$ $\frac{1}{2} \left[\frac{-2k_{IMM} K_{IMM} \bar{C}_b}{(K_{IMM} + \bar{C}_b)^3} \right] \sigma_{\bar{C}_b}^2 +$ $\left[\frac{k_{IMM} K_{IMM}}{(\bar{C}_b + K_{IMM})^2} \right] \bar{C}'_s \bar{C}'_b$	Eq. (A10)	Eq. (A10)

* The expression of \bar{D} for multiplicative kinetics in each heterogeneity case is exact.

To summarize, we started with the spatial averaging of the SOM dynamics equations at micro-scale and applied scale transition theory to derive relations between the micro- and macro-scale C fluxes, which depend on both mean state variables and their spatial statistics (Table 2). Thus, to solve the macro-scale Eqs. (13) and (14), we still need information regarding the second order moments i.e., $\sigma_{\bar{C}_s}^2$ and $\bar{C}'_s \bar{C}'_b$. To close the problem mathematically, these moments can be regarded as extra state variables requiring additional differential equations to describe their dynamics (Keeling et al., 2002; Murrell et al., 2004; Barraquand and Murrell, 2013). Alternatively, the second order moments can be parameterized as empirical functions of first order terms \bar{C}_s , \bar{C}_b and \bar{k} (Bergström et al., 2006). Here, our goal is to quantify how heterogeneities alter C fluxes in idealized systems, so we leave the closure problem for a future contribution and use instead the numerically simulated dynamics at the micro-scale to calculate the spatial moments and SOT.

10 2.3 Model setup

As in previous spatially explicit models (Ginovart and Valls, 1996; Allison, 2005; Kaiser et al., 2014), we start with a 2D domain characterized by an initial heterogeneous field of the substrate and numerically simulate the dynamics of SOM with

the micro-scale two pool model in Eqs. (2)–(4) at each cell in the domain. The 2D domain has 100×100 square grid cells with an edge length of $50 \mu\text{m}$, and we populate it with randomly generated initial substrate fields. This numerical model is referred to as ‘distributed model’ (see, Fig. 1). From the solution of the distributed model, the mean behavior of the system ($\overline{C_s}, \overline{C_b}, \overline{D}, \sigma_{C_s}^2, \sigma_{C_b}^2$, and $\overline{C'_s C'_b}$) can be calculated at each time step by using sample statistics of C_s and C_b

$$5 \quad \overline{C_s}(t) \approx \frac{1}{N_x N_y} \sum_{i=1}^{N_x} \sum_{j=1}^{N_y} C_{s_{i,j}}(t), \quad (24)$$

$$\overline{C_b}(t) \approx \frac{1}{N_x N_y} \sum_{i=1}^{N_x} \sum_{j=1}^{N_y} C_{b_{i,j}}(t), \quad (25)$$

$$\overline{D}(t) \approx \frac{1}{N_x N_y} \sum_{i=1}^{N_x} \sum_{j=1}^{N_y} k_{M_{i,j}} C_{s_{i,j}}(t) C_{b_{i,j}}(t), \quad (26)$$

$$\sigma_{C_s}^2(t) \approx \frac{1}{N_x N_y} \sum_{i=1}^{N_x} \sum_{j=1}^{N_y} [C_{s_{i,j}}(t) - \overline{C_s}(t)]^2, \quad (27)$$

$$\sigma_{C_b}^2(t) \approx \frac{1}{N_x N_y} \sum_{i=1}^{N_x} \sum_{j=1}^{N_y} [C_{b_{i,j}}(t) - \overline{C_b}(t)]^2, \quad (28)$$

$$10 \quad \overline{C'_s C'_b}(t) \approx \frac{1}{N_x N_y} \sum_{i=1}^{N_x} \sum_{j=1}^{N_y} [C_{s_{i,j}}(t) - \overline{C_s}(t)] [C_{b_{i,j}}(t) - \overline{C_b}(t)], \quad (29)$$

where \overline{D} is specified for multiplicative kinetics; a similar approach was applied for MM and IMM kinetics. Table A1 in the appendix lists all the parameters related to different kinetic models used in the simulations. We performed the simulations in mass units fg (fg = 10^{-15} g) and later converted the state variables to concentration units i.e. mgC/g of soil.

2.4 Initial 2D random fields of SOM and kinetic parameters

15 Two-dimensional spatially heterogeneous distributions of substrates and microbial C were generated to run the distributed model. The obtained distributions were based on the following constraints: i) the total amount of organic C is set, ii) the total amount of microbial C is 1% of total organic C, iii) the maximum amount of C in a cell is set (Eq. (A12)), and iv) some grid cells have no microbial biomass. For details on the spatial field generation, see Appendix A2.

To study the effects of the degree of heterogeneity on decomposition, random fields of substrate C with different degrees of 20 correlation with microbial C were generated. We created three cases where substrate and microbial C were initially positively correlated, negatively correlated or uncorrelated. The three cases were obtained by applying a linear operator on the microbial C fields with positive and negative slope to obtain positively and negatively correlated substrate C fields, respectively. The

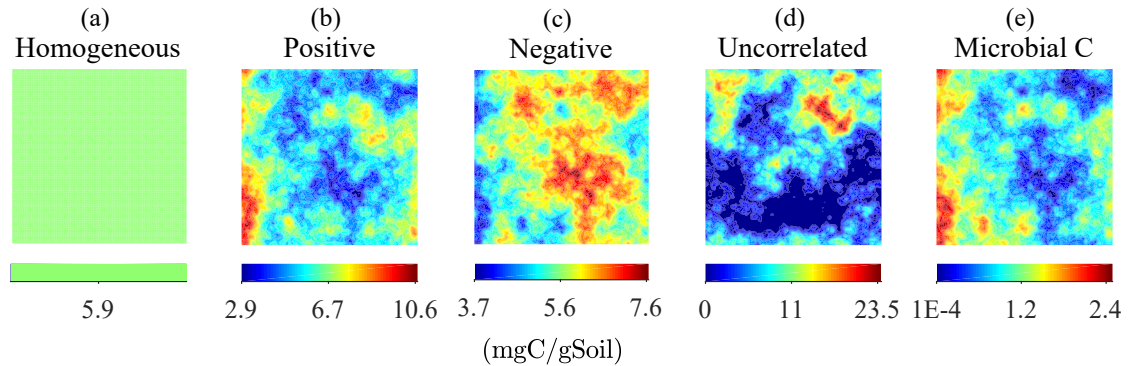


Figure 2. Steady state simulation: Examples of the homogeneous (a) and the heterogeneous distributions of substrate C constrained to have the same total amount of substrate C (b–d). The fields in b–d were obtained by imposing different degrees of correlation with the initial heterogeneous distributions of microbial C, shown in (e).

uncorrelated substrate C field was generated independently from the microbial C field and can be interpreted as the result of external disturbances disrupting preexisting spatial correlations. The case of positive initial correlation between substrate and microbial C would result in a heterogeneous system with spatial co-occurrence of substrate and microbial C, whereas initial negative correlation would result in isolated patches of substrate and microbial C. In all scenarios, the substrate distributions are normalized to have the same amount of total substrate C, thereby allowing for comparisons among different degrees of heterogeneity (Figure 2).

To generate a heterogeneous random field for kinetic parameters, we considered a uniform distribution for K_{MM} and K_{IMM} , and a log-uniform distribution for k_M , k_{MM} , and k_{IMM} (Forney and Rothman, 2012; Manzoni et al., 2012). The log-uniform distributions were defined so that the mean kinetic constants were equal to those of the homogeneous system (Table A1) and their variances were tuned to characterize different degrees of heterogeneity. To generate the initial fields, $N_x \times N_y$ random numbers were extracted from the chosen distributions and placed into the 2D domain. Figure A7 in the appendix shows the probability densities for two different standard deviations for k_{MM} and k_M (the parameters of the distributions are listed in Tables A2 and A3).

2.5 Estimation of kinetic parameters

To choose parameter values for the linear and multiplicative kinetics that allow comparisons with the MM model, we first simulated the substrate C dynamics at micro-scale for a given initial condition and using MM kinetics. Second, we fit the linear and multiplicative kinetics models to the time series obtained using MM kinetics (using the optimization toolbox in MATLAB). In this procedure, we assumed that the microbial mortality constant (k_B) was the same for all choices of the decomposition

model. The parameters of the inverse MM are chosen (by trial and error) so that the respiration rate in the homogeneous system is comparable to that in the heterogeneous system.

2.6 Simulation scenarios

Two scenarios, based on varying initial conditions (IC) were implemented to investigate the effects of micro-scale hetero-
5 geneities on macroscopic decomposition (Fig. 3).

Scenario 1 (steady state simulation - SS): In this scenario, the initial heterogeneous field of substrate and microbial C was generated as described in section 2.4. The spatial mean of the initial substrate and microbial C match their steady state values given by the micro-scale equations (Eqs. (5) and (6)) forced with a constant substrate input. Additionally, a minimum amount of microbial C was set in each cell (values at least one order of magnitude lower than those at steady state) to ensure that OM
10 could be decomposed, albeit at a slower rate than elsewhere.

Scenario 2 (high substrate simulation - HS): In the scenario, the initial heterogeneous field of substrate C was perturbed around a value much larger than the steady state as described in section 2.4.

In the HS scenario, simulations were based on three nonlinear decomposition models (multiplicative, MM, and IMM kinetics). However, in the SS scenario, we present results only for multiplicative kinetics because MM kinetics can be approximated
15 by multiplicative kinetics when the substrate is much smaller than the half-saturation constant (K_{MM}), as is the case with the chosen initial heterogeneous substrate field and the values of K_{MM} . Results using the linear decomposition model are not shown because with this model the spatially-averaged fluxes are equal to the macro-scale flux calculated at the mean C concentration (Eq. (17)), as long as k_L is homogeneously distributed.

In both scenarios, we explore the effects of biophysical and full heterogeneity on the temporal evolution of the mean state
20 variables (substrate and microbial C) and their associated rates. We used the distributed model to estimate the mean quantities and second order spatial moments (and thus SOT) for three degrees of biophysical heterogeneity. A homogeneous system in which the initial substrate and microbial C, as well as kinetic parameters, are spatially uniform was always used as a control. The combined effect of biophysical and biochemical heterogeneity was simulated by imposing the spatially heterogeneous kinetic parameters along with the heterogeneous initial substrate and microbial C.

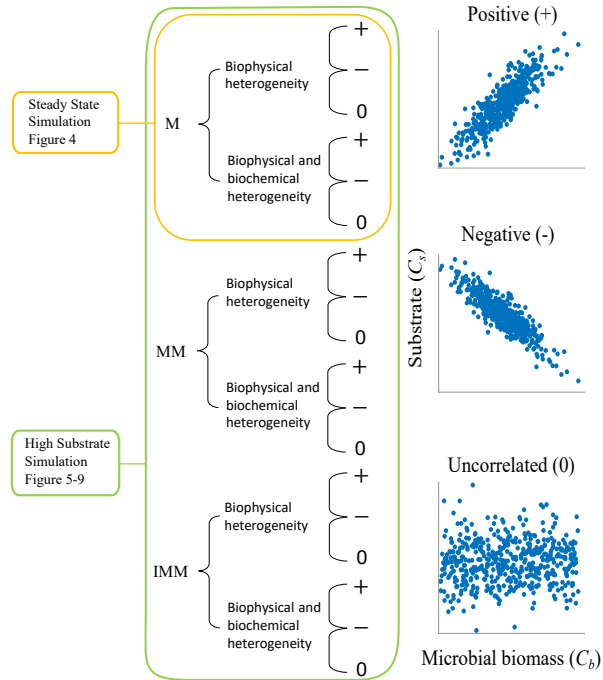


Figure 3. Two scenarios were implemented based on initial spatial distribution of substrate and microbial C. In scenario 1, substrate and microbial C are perturbed around the steady state of the micro-scale differential equations and simulations are only carried out with the multiplicative (M) kinetics. In scenario 2, substrate and microbial C are perturbed to values larger than the steady state, and simulations are conducted for multiplicative (M), Michaelis-Menten, (MM) and inverse Michaelis-Menten (IMM) kinetics. For each scenario and type of heterogeneity, three different initial distributions of substrate and microbial biomass are considered as representative of micro-scale heterogeneities (positively correlated (+), negatively correlated (-), and uncorrelated (0) fields of substrate and microbial C).

3 Results

3.1 Scenario 1: steady state simulation (SS)

Figure 4 illustrates the temporal evolution of the macroscopic decomposition dynamics for the three different heterogeneous cases with varying degrees of initial correlation between substrate and microbial C in comparison to the homogeneous system.

- 5 In figure 4, the left and right panels respectively show the effects of biophysical heterogeneity and full heterogeneity on the mean C pools and fluxes (k_M is based on the case 'biochemical heterogeneity 1' in Table A3). For this analysis, we focus on the multiplicative decomposition model. With the current parameter choice, the ratio of microbial biomass to substrate C attains at steady state values that are larger than would be expected for biomass-to-total SOC ratios (Xu et al., 2013). This is due to our interpretation of substrate C as a relatively active fraction of total SOC.

Since the mean initial condition corresponds to the steady state of the micro-scale system, in a homogeneous soil no changes occur in substrate C (solid line in Figs. 4a and 4b) and microbial C (solid line in Figs. 4c and 4d), and the mean respiration rate is equal to the constant rate of input of external C (solid line in Figs. 4e and 4f). In contrast, for the system with biophysical heterogeneity, the mean C pools and respiration (\bar{R}) fluctuate towards the steady state of the micro-scale system as a result of the heterogeneous initial placement of C substrates. Similarly, for the fully heterogeneous system the mean microbial C pool (Fig. 4d) and fluxes (Fig. 4f) fluctuate near their steady state values, but the mean substrate C pool (Fig. 4b) reaches a new steady state. The value of the new steady state for the \bar{C}_s depends upon the parameters of the log-uniform distribution of k_M and is given the Appendix A3.

In all heterogeneity scenarios, \bar{R} is initially higher than in the homogeneous system when substrate and microbial C are initially correlated, whereas it is lower when substrate and microbial C are negatively correlated. When substrate and microbial C are uncorrelated, the system exhibits a behavior similar to that of the positively correlated fields, but with higher respiration peaks (Fig. 4e). This is caused by the high initial spatial variance of substrate C that resulted in hot spots richer in substrate C than in the positively correlated case (Fig. 2). Furthermore, in the multiplicative kinetics, the respiration flux is proportional to the amount of substrate C, so that larger variations in substrate cause larger fluctuations in the mean respiration flux. In the fully heterogeneous system, fluxes show similar dynamics as those in the biophysically heterogeneous system, except for the different steady state. Varying the mean (Fig. A1) and variability (Fig. A2) of k_M alters the quantitative, but not qualitative, behavior of the macro-scale system (results shown in Appendix A4).

Figure 4g and 4h show the sum of all higher order terms ($\sum HOT$, see Table 2 for multiplicative kinetics). For a biophysically heterogeneous system, the $\sum HOT$ only includes the spatial covariance term (Eq.(18)), but for a fully heterogeneous system it includes the last three terms of the Eq. (21) as well as the third order term $\overline{k'_M C'_s C'_b}$. The $\sum HOT$ is initially positive, zero and negative, respectively for positively correlated, uncorrelated, and negatively correlated substrate and microbial C, and exhibits strong temporal variations (Fig. A3). A positive $\sum HOT$ value enhances \bar{R} , whereas a negative value decreases it in all three heterogeneous cases compared to homogeneous \bar{R} . This result is aligned with our expectation from the analytical expression of the macro-scale multiplicative model. In systems including both biophysical and full heterogeneity, the sums of the HOT are stable in the long term, once the steady state has been reached. This was confirmed by running the model for 100 years. Furthermore, any additional perturbation of the new steady state caused by an external factor will re-introduce these fluctuations.

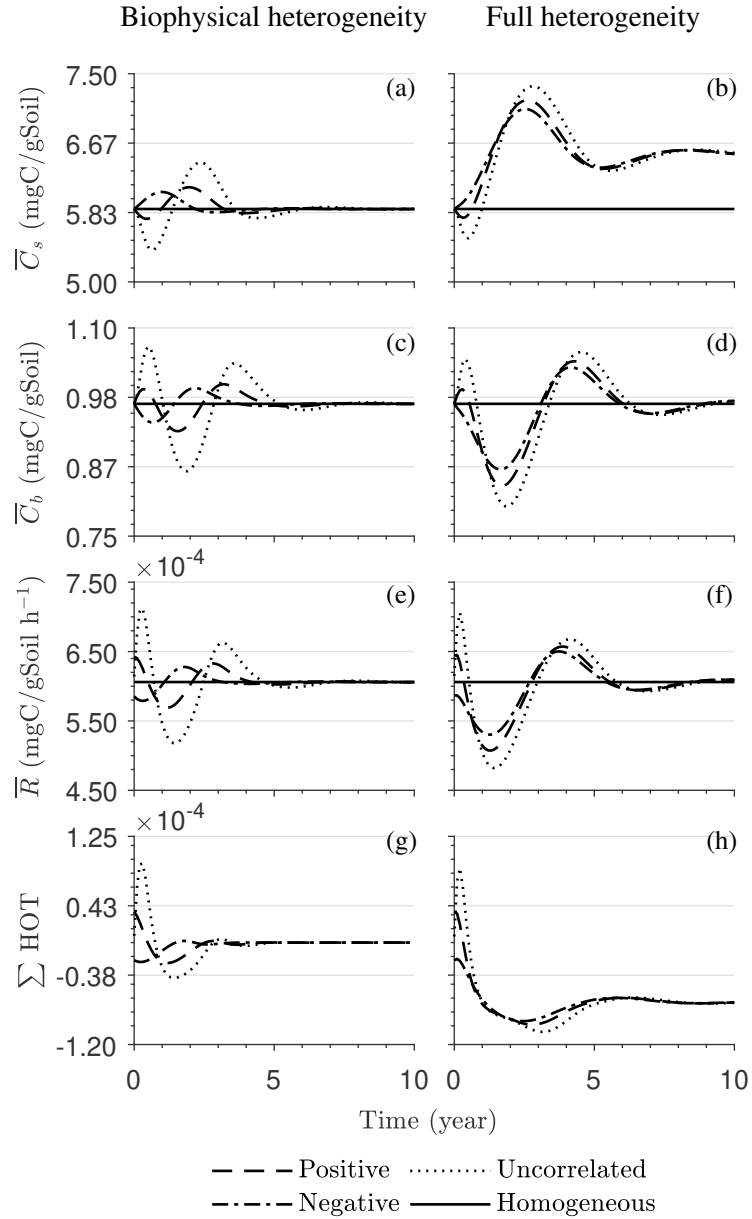


Figure 4. Scenario 1 (steady state simulation): effect of biophysical (left panel) and full heterogeneity (right panel) on the macroscopic decomposition dynamics when the substrate is distributed randomly around the steady state, and only considering multiplicative kinetics at the micro-scale: (a,b) mean substrate C (\bar{C}_s), (c,d) mean microbial C (\bar{C}_b), (e,f) mean respiration rate (\bar{R}), and (g,h) sum of second and third order terms ($\sum HOT$).

3.2 Scenario 2: high substrate simulation (HS)

3.2.1 Dynamics of substrate and microbial C at the macro-scale

Figure 5 illustrates the temporal evolution of the mean properties of the macroscopic decomposition dynamics for multiplicative kinetics, for systems with either biophysical (left panel) or full (right panel) heterogeneity, when the initial condition is perturbed from the steady state by adding C substrates. In this scenario, both homogeneous and heterogeneous systems exhibit transient dynamics because the initial conditions are set far from the steady state. The results in Fig. 5c indicate that, during the microbial growth phase, the production of microbial C is faster when substrate and microbial C are positively correlated or uncorrelated, compared to the case of negative correlation. Consequently, at the beginning of the simulation, the mean substrate \bar{C}_s (Fig. 5a) is decomposed faster due to the higher respiration (Fig. 5e) for the positively correlated and the uncorrelated substrate and microbial C, and slower for the negatively correlated substrate and microbial C, when compared to the homogeneous system. By the end of the simulation period, in all heterogeneous scenarios, biomass production and substrate consumption are lower than in the homogeneous system. As in scenario 1, the initial mean respiration for the uncorrelated case is higher than that in the positively correlated case. Moreover, the fully heterogeneous system (Fig. 5 right panels) shows a similar behavior as the biophysically heterogeneous system, but the peaks of \bar{R} appear earlier for all degrees of correlation between substrate and microbial C.

Similar to Fig. 4, Figs. 5g and 5h show the sum of all higher order terms (see Table 2, multiplicative kinetics). For both heterogeneous systems, \bar{R} is higher than the MFA when the $\sum HOT$ is positive, whereas \bar{R} is lower than the MFA when the contribution of these moments is negative. This result agrees with the analytical expression and is valid for all types of biophysical heterogeneities. The $\sum HOT$ for biophysical heterogeneity is initially positive for the positively and the uncorrelated substrate and microbial C, but later becoming negative, whereas it is always negative for the negatively correlated substrate and microbial C. Spatial covariances among kinetic parameter and state variables (i.e., $\overline{k'_M C'_s}$, $\overline{k'_M C'_b}$, $\overline{k'_M C'_s C'_b}$) also contribute to the $\sum HOT$ in the fully heterogeneous system in addition to $\overline{C'_s C'_b}$. Specifically, the spatial covariance between k_M and C_b gives rise to early peaks of \bar{R} (see all HOT in Fig. A4).

Figures 6 and 7 show similar results as Fig. 5, but for Michaelis-Menten and inverse Michaelis-Menten kinetics, respectively. The transient dynamics of the mean C pools and fluxes differ from those obtained using multiplicative kinetics. For both MM and IMM kinetics, during the initial growth period, the mean respiration rate in the biophysically heterogeneous systems is similar to that occurring in a homogeneous system, but \bar{R} attains lower peaks (Figs. 6e and 7e). As a result, substrate loss (Figs. 6a and 7a) and microbial growth (Figs. 6c and 7c) slow down compared to homogeneous conditions. Interestingly, with

MM kinetics, in the uncorrelated case \bar{R} is not higher than in the other heterogeneity cases as occurred with multiplicative kinetics (compare Figs. 6e and 5e). This is because with MM kinetics the respiration flux is limited by the maximum rate of decomposition and not only by substrate availability. In contrast, with IMM kinetics \bar{R} in the uncorrelated case is higher than in the other heterogeneity cases, as it was with multiplicative kinetics. This is because the initial microbial C is often much lower than the half saturation constant for IMM kinetics, making the IMM decomposition rates numerically similar to those obtained using the multiplicative decomposition model.

The fully heterogeneous system (right panels in Figs. 5, 6, and 7) shows different behavior compared to the biophysically heterogeneous system. The peaks of \bar{R} appear much earlier than in the biophysically heterogeneous system, though the temporal shift of the peak is not as pronounced with IMM kinetics. Additionally, the values of mean fluxes and C pools after the peak are respectively smaller and larger than in the homogeneous system or the system with only biophysical heterogeneity. The smaller mean fluxes are due to the left skewed probability distribution of the kinetic parameters (k_M and k_{MM}), which causes slower decay despite the mean values of the kinetic parameters being the same. Mathematically, this behavior is caused by the additional covariances in the fully heterogeneous system as explained in the following paragraph.

3.2.2 Dynamics of the second order terms

The $\sum SOT$ (same as $\sum HOT$ but now limiting the HOTs to second order) for MM and IMM kinetics for the biophysically heterogeneous system is given by the sum of the last two terms of \bar{D} in Table 2 and for the fully heterogeneous system it is given by the last eight terms of Eq. (A9) and Eq. (A10), respectively. For the biophysically heterogeneous system, the values of $\sum SOT$ (Figs. 6g and 7g) are initially positive (very small in magnitude) for the positively correlated substrate and microbial C and later become negative, while for the negatively correlated heterogeneous case $\sum SOT$ is always negative. For uncorrelated substrate and microbial C, $\sum SOT$ is initially negative in MM kinetics but mildly positive in IMM kinetics and later becomes negative. Furthermore, the balance between variance and covariance terms makes the MFA a good approximation of \bar{R} only when the combined second order terms are negligible, which is not the case in this example (see, Figs. A5 and A6). The $\sum SOT$ of the fully heterogeneous system for MM kinetics is positive for the first 100 days of simulation and then negative onward, even though the heterogeneous \bar{R} is smaller than the homogeneous \bar{R} (Fig. 6h). This initial positive $\sum SOT$ is driven by the sixth SOT in Eq. (A9) i.e. $\frac{\partial^2 F}{\partial k_{MM} \partial C_b} \Big|_{\bar{C}_s, \bar{C}_b, \bar{k}_{MM}, \bar{K}_{MM}} \overline{C'_b k'_{MM}}$, because grid cells with high amount of microbial C and high rate constant give the covariance $\overline{C'_b k'_{MM}}$ to be positive. This covariance becomes negative only after microbial C nears the steady state.

3.2.3 Emerging macroscopic kinetics

Figure 8 highlights the effects of spatial heterogeneities on the mean specific growth rate (SGR) for multiplicative (top), MM (middle), and IMM kinetics (bottom panels). The depicted SGR curves can be interpreted as the macroscopic kinetic laws emerging from the spatial averaging. For all three kinetics, the functional relation between the mean SGR and \bar{C}_s for the heterogeneous system depends upon the initial degree of heterogeneity. In contrast, in the homogeneous system the mean SGR is a linear, saturating, and exponentially increasing function of C_s for the multiplicative, MM, and IMM kinetics, respectively. The effect of biophysical heterogeneity in all kinetic models are shown in Figs. 8a, 8c and 8e. The negative correlation between substrate and microbial C leads to lower SGR than in the homogeneous system, even if both heterogeneous and homogeneous systems have exactly the same amount of total initial substrate and microbial C. In the case of positive correlation, the initial mean SGR is higher than in the homogeneous system, but in the later phase of decomposition, mean SGR becomes lower. Thus, when the substrate is co-located with the microorganisms, the mean SGR is initially higher but it decreases at a faster rate as the substrate is decomposed when compared to the homogeneous system. If substrate and microbial C are uncorrelated, the SGR functional response remains between the negative and the positive correlation cases.

In the fully heterogeneous system (Figs. 8b, 8d, and 8f), the nonlinear character of the relation between mean SGR and \bar{C}_s increases compared to the biophysically heterogeneous system. Interestingly, the mean SGR in the case of negative correlation for multiplicative and MM kinetic models is higher (for high \bar{C}_s) than for the homogeneous system, despite being the co-location of substrates and microorganisms less likely. This behavior is caused by the occurrence of patches with high turnover rate that control the mean SGR (Figs. 8a and 8c). In contrast, for IMM kinetics, the mean SGR in the case of negative and positive correlation is lower than the homogeneous system. This behavior might be a consequence of the chosen value of K_{IMM} ; i.e., in our parameterization of the IMM kinetics, initially the system is limited by microbial C, resulting in relatively low decomposition rate and dynamics comparable to those obtained with a multiplicative model (see, Fig. 7e-f).

In Fig. 9, we show the specific growth rate as a function of substrate for an uncorrelated initial distribution of substrate and microbial C, and for all three kinetics– multiplicative, Michaelis-Menten and inverse Michaelis-Menten. When $\alpha = 0$, result in Fig. 9 are same as in Fig. 8 for the uncorrelated case. When $\alpha > 0$, microorganism that were initially deprived of substrate now receive additional substrate from neighboring grid cells. As a consequence of this improved substrate availability, in long-term microorganisms can consume all the substrate, whereas without mass transfer some C remains undecomposed (Figs. 5b, 6b, and 7b).

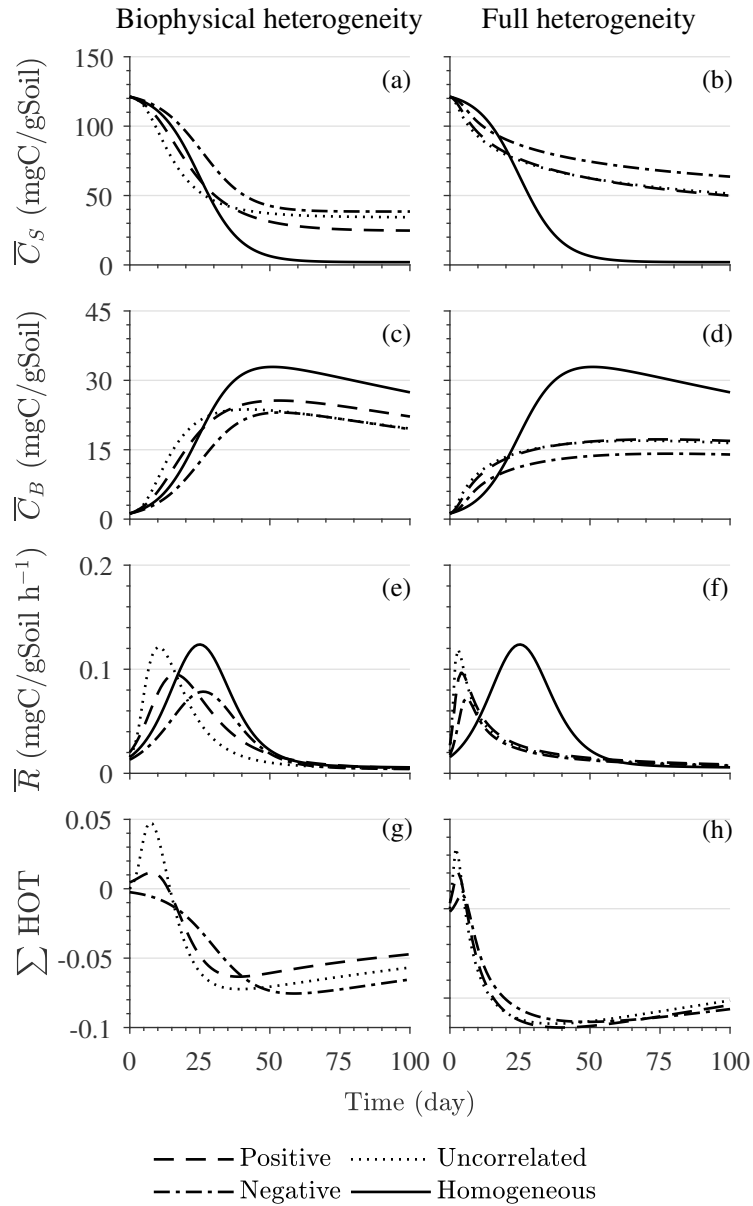


Figure 5. Scenario 2 (HS with multiplicative kinetics): effect of biophysical heterogeneity (left panel) and full heterogeneity (right panel) on the macroscopic decomposition dynamics when the substrate is distributed around a value higher than the steady state of the homogeneous system: (a,b) mean substrate C (\bar{C}_s), (c,d) mean microbial C (\bar{C}_b), (e,f) mean respiration rate (\bar{R}), and (g,h) sum of second and third order terms ($\sum HOT$).

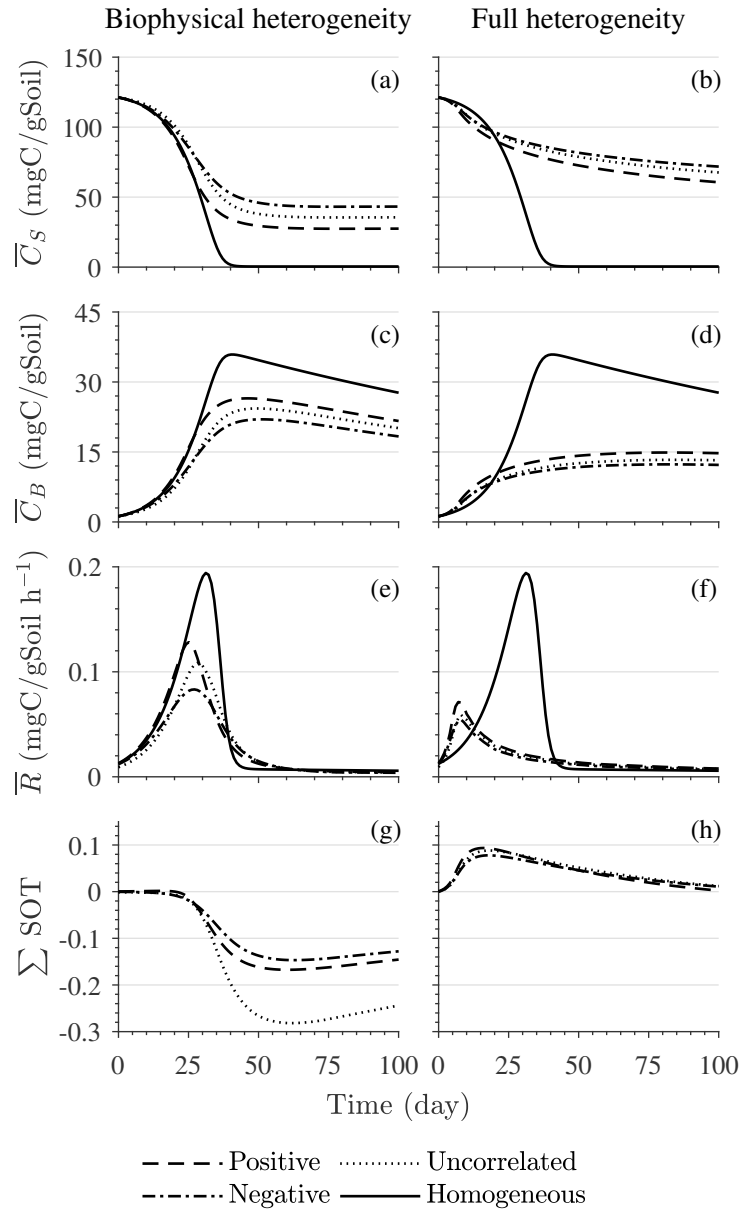


Figure 6. Scenario 2 (HS with Michaelis-Menten kinetics): effect of biophysical heterogeneity (left panel) and full heterogeneity (right panel) on the macroscopic decomposition dynamics when the substrate is distributed around a value higher than the steady state of the homogeneous system: (a,b) mean substrate C (\bar{C}_s), (c,d) mean microbial C (\bar{C}_b), (e,f) mean respiration rate (\bar{R}), and (g,h) sum of second order terms ($\sum HOT$).

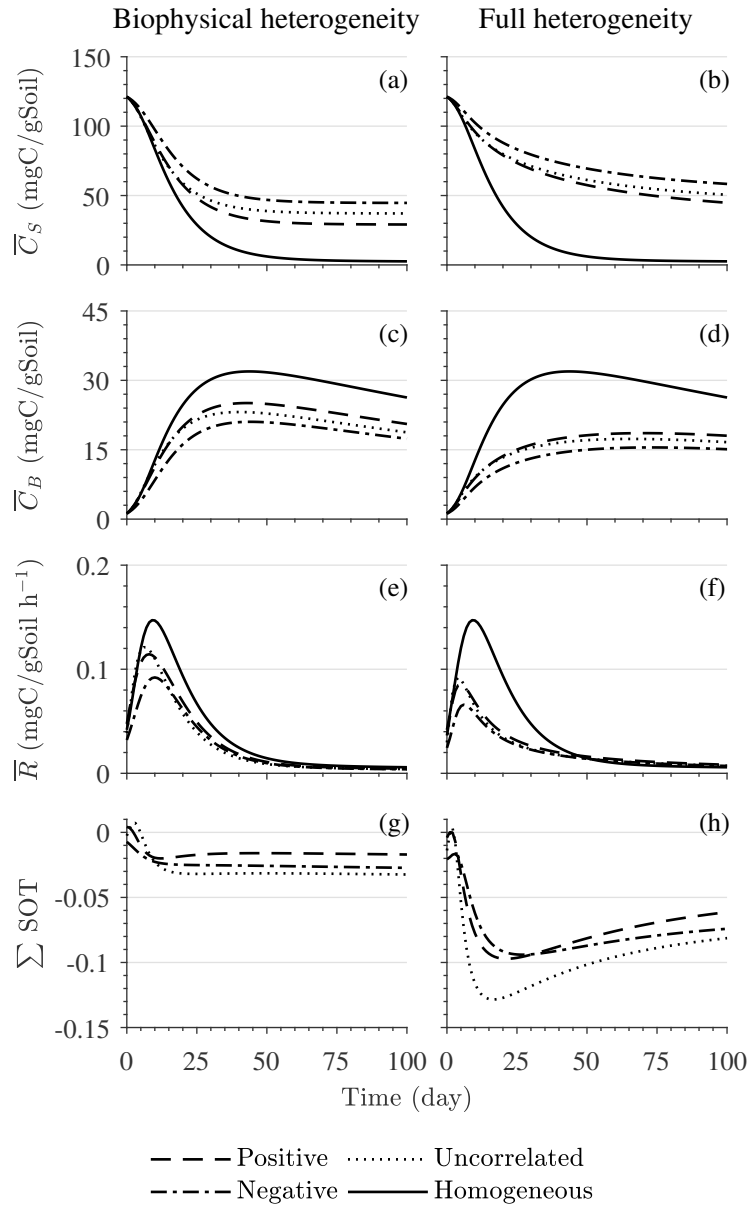


Figure 7. Scenario 2 (HS with inverse Michaelis-Menten kinetics): effect of biophysical heterogeneity (left panel) and full heterogeneity (right panel) on the macroscopic decomposition dynamics when the substrate is distributed around a value higher than the steady state of the homogeneous system: (a,b) mean substrate C (\bar{C}_s), (c,d) mean microbial C (\bar{C}_b), (e,f) mean respiration rate (\bar{R}), and (g,h) sum of second order terms ($\sum HOT$).

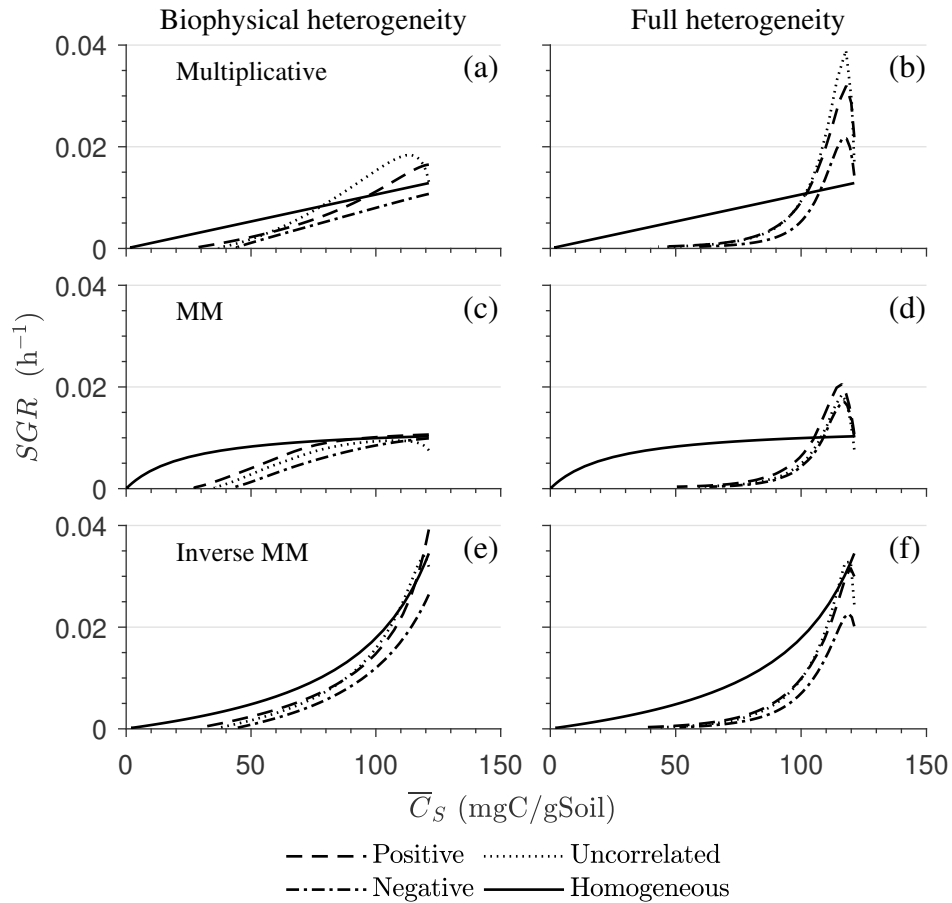


Figure 8. Effect of spatial heterogeneity on the mean specific growth rate (SGR) for HS scenario with the simplified micro-scale model (no C redistribution): Effect of biophysical (left column) and full (right column) heterogeneity on the mean SGR as a function of mean substrate C (\bar{C}_s) for the heterogeneous system for (a,b) multiplicative, (c,d) Michaelis-Menten, and (e,f) inverse Michaelis-Menten kinetics. Time progresses from right to left, as \bar{C}_s is depleted.

4 Discussion

4.1 Predicted effects of spatial heterogeneity on decomposition

The heterogeneous spatial distribution of organic matter in soils is a result of complex physical, chemical, and biological processes. Both the experimental quantification of the effects of heterogeneity on SOM dynamics (Kravchenko and Guber, 2017), and capturing such effects in mathematical models (Wieder et al., 2015) is challenging. Here, we used scale transition theory, applied to a two pool model, as a simple approach to analytically account for spatial heterogeneities and upscale SOM dynamics in idealized scenarios that cover different types of spatial heterogeneity. Even with the simplest scenarios, the macroscopic

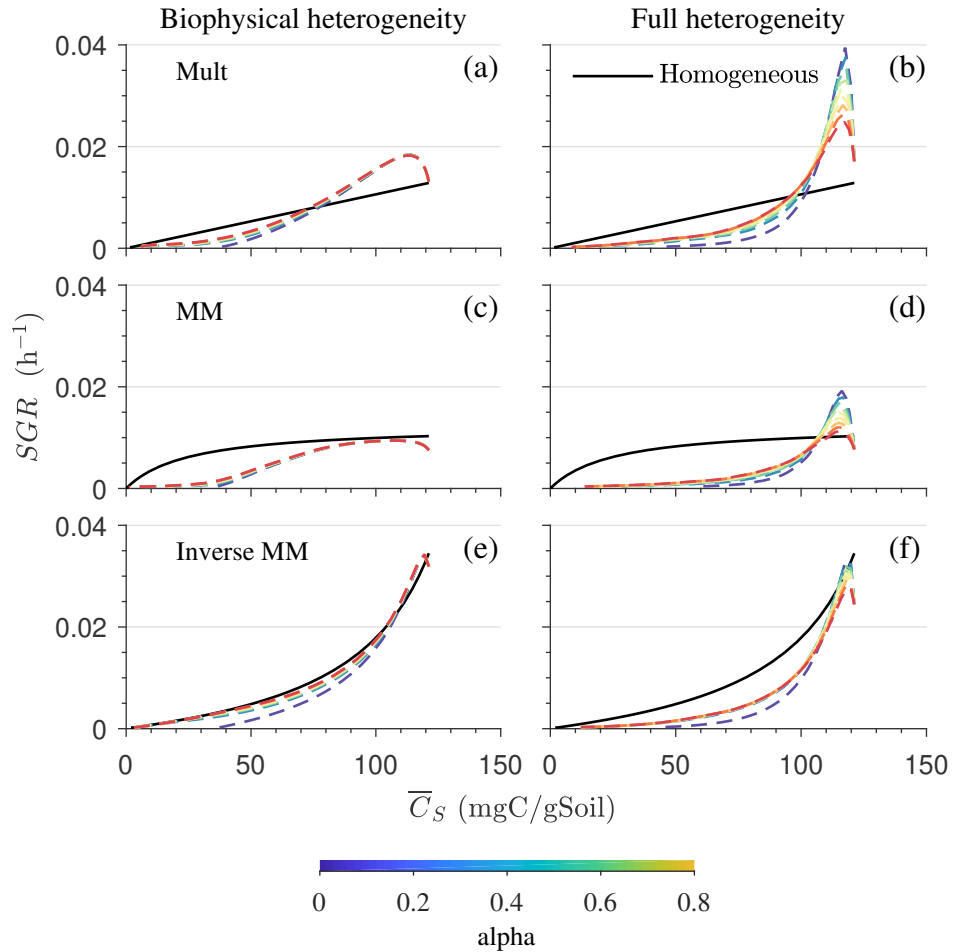


Figure 9. Effect of spatial heterogeneity on the mean specific growth rate (SGR) for HS scenario including C redistribution : Effect of biophysical (left column) and full (right column) heterogeneity on the mean SGR as a function of mean substrate C (\bar{C}_s) for an uncorrelated initial distribution of substrates and microorganisms. The three horizontal panels are for (a,b) multiplicative, (c,d) Michaelis-Menten, and (e,f) inverse Michaelis-Menten kinetics. Different colors represent varying values of α . Time progresses from right to left, as \bar{C}_s is depleted.

decomposition dynamics of a heterogeneous system differ from those predicted from the mean-field approximation (equivalent to assuming well-mixed conditions). This difference in the dynamics at two spatial scales arises because spatial averaging of the nonlinear kinetics at the micro-scale create additional terms in the macro-scale equations that depend on the spatial distribution of organic matter and microorganisms (i.e., the second order spatial moments, SOT).

5 These second order terms represent corrections to the mean-field approximation and depend on the spatial variability and co-variation of the state variables (i.e. C_s and C_b). Our numerical results showed that the second order spatial moments have their own dynamics that drive the heterogeneous system away from the mean-field approximation. Notably, while it is recognized that spatial distributions at the micro-scale affect macro-scale dynamics (Falconer et al., 2015), none of the current spatially-lumped SOM models include second or higher order terms that depend on micro-scale heterogeneity (see Sect. 4.3).

10 The simplicity of the micro-scale model and the derived analytical expressions are such that specific insights on how heterogeneity shapes micro-scale decomposition patterns can be gleaned and hypotheses generated. The main predictions of this model are

1. Perturbing a system that is initially homogeneous and at steady state by redistributing substrates triggers fluctuations around the steady state (Fig. 4).
- 15 2. When only biophysical heterogeneity occurs, in the early microbial growth phase, macroscopic C fluxes are enhanced by the co-location of substrates and microorganisms, and reduced when they are isolated (Figs. 8a–c).
3. Combined biophysical and biochemical heterogeneity enhance C fluxes in the early stage of decomposition but reduce them in the later stages, compared to a homogeneous system (Figs. 8b–d).
4. Both biophysically and fully heterogeneous systems result in a transient persistence of SOM (Figs. 5a,d and 6a,d). In the
20 biophysically heterogeneous system at steady state, all C is eventually decomposed, whereas in the fully heterogeneous system more C is retained as the substrate pool reaches a new equilibrium (Appendix A3).
5. For a successive reduction in the degree of heterogeneity (i.e. systematically moving from a heterogeneous to a homogeneous system), macro-scale dynamics converge to the mean-field approximation; i.e., the same kinetics can be used at all scales (Sect. 2.1.2).
- 25 6. Increasing local connectivity among grid cells moderately reduces the effect of spatial heterogeneity on the macro-scale variables and fluxes.

7. The inverse Michaelis-Menten kinetics appear to be less sensitive to the scale transition than multiplicative and Michaelis-Menten kinetics, but this result might depend on the specific choice of parameter values (for a discussion on scale invariance of upscaled kinetics for reaction networks, see (Tang and Riley, 2017)).

Our analysis suggests that the persistence of SOM in heterogeneous systems may be a consequence of the micro-scale heterogeneity in soil carbon cycling. In the transient simulations with biophysical heterogeneity, persistence is a result of spatial disconnection between substrate and microorganism, captured in our framework by a low probability of co-location at the beginning of the simulation. In the transient simulations for the fully heterogeneous systems, persistence is a result of the combined effects of low probability of co-location and high probability of low decomposition rate constant at the beginning of the simulation. The heterogeneity in substrate quality thus explains the higher persistence of SOM in the fully heterogeneous system compared to the biophysically heterogeneous system.

4.2 Linking theory and observations

We studied three initial heterogeneous distributions of substrate and microbial C; positive, negative or no correlation between these two variables. These heterogeneities may correspond to spatial aggregation, isolation or random occurrence of substrate and microorganisms, respectively. Spatial aggregation is expected in litter and in the surface soil where substrate is abundant and microbial colonies are formed around hot spots (Nunan et al., 2003). Spatial isolation is more likely to occur in the subsoil because of lower substrate and microorganism density as well as poor pore connectivity (Ekschmitt et al., 2008; Salomé et al., 2010), and C-rich patches occur around roots that are separated by large (in a relative sense) volumes of soil that only receive diluted resources via percolation, diffusion, and bioturbation (Kuzyakov and Blagodatskaya, 2015). Uncorrelated spatial fields of substrate and microorganisms may correspond to spatial distributions between these two extremes. There are other examples of contrasting homogeneous vs. heterogeneous conditions. Disturbed, sieved or dispersed samples may be considered as homogeneous, whereas intact soil samples retain their natural heterogeneity.

Despite the correspondence of our idealized heterogeneity scenarios with conditions in natural soils or soil samples, linking our model predictions to observations is challenging, mostly because the effects of heterogeneity can not be easily isolated in experiments or field observations. Experiments studying the effects of soil structure on the dynamics of SOM mineralization may introduce other types of heterogeneities that are not dealt with here. For example, samples with different pore networks likely exhibit different water and air diffusive pathways, which in turn affect microbial respiration (Killham et al., 1993; Stenger et al., 2002; Ruamps et al., 2011; Juarez et al., 2013; Negassa et al., 2015; Herbst et al., 2016) (Manzoni and Katul, 2014; Herbst et al., 2016; Koestel and Schlüter, 2019). When targeting experiments to test our up-scaled

equations, using data from previous studies is challenging because (i) spatial distribution of substrate and/or microbial C are not changed in a controlled manner and (ii) the scale at which physical treatments are performed is probably larger than the scale at which heterogeneity affects C dynamics.

Thus, experiments in which soil structure was manipulated do not allow direct testing of the predicted links between heterogeneity and decomposition kinetics at the macro-scale. Further, an experimental validation of the present work should stem from designing a micro-scale experiments using artificial porous media with different degrees of heterogeneity. Recent application of microfluidics in soil science (Stanley et al., 2016; Aleklett et al., 2018) could allow isolating the effect of spatial heterogeneity. If any difference is observed among heterogeneous systems, then our framework could be used to attribute these differences to spatial heterogeneity at the micro-scale. While the proposed mathematical framework is conceptually useful, it is thus challenging to test. Nevertheless, the prediction that co-location of microorganisms and substrates promotes decomposition is consistent with and explains theoretically the results of recent experiments (Don et al., 2013; Schneckner et al., 2019).

4.3 Developing soil carbon cycling models that account for micro-scale heterogeneity

Historically, the linear microbial implicit models were developed to explain long-term loss of C from agricultural soils or regional-scale variations in SOM (Jenny et al., 1949; Olson, 1963; Jenkinson and Rayner, 1977; Parton et al., 1987). However, when applied at fine spatial or temporal scale, these models fail to describe the dynamics of SOM (Zelenev et al., 2000; Manzoni and Porporato, 2007). To fill this gap and describe microbial processes at the macro-scale, nonlinear microbial explicit models have been proposed (Schimel and Weintraub, 2003; Manzoni and Porporato, 2009; Xie, 2013). In contrast to these approaches that impose nonlinear kinetics at the macro-scale, here we started from the assumption that SOM kinetics are either linear or nonlinear at the micro-scale, and let scale transition theory determine the type of kinetics at the macro-scale.

Conceptually, this approach is similar to upscaling chemical reaction networks to obtain a compact kinetic law that only depends on the concentrations of reactants and products (Tang and Riley, 2013, 2017). However, here we focus on spatial heterogeneity rather than on the complexity of chemical reactions. In a more complete upscaling approach, both sources of micro-scale variability should be taken into account.

When assuming linear kinetics at the micro-scale, we showed analytically that the kinetics at the macro-scale remain linear and independent of soil biophysical heterogeneity (Eqs. (17) and (22)). This result has implications for experimental studies linking soil architecture to SOM mineralization. In some of these studies, first order microbial implicit kinetics are used to describe the data (Bouckaert et al., 2013; Juarez et al., 2013). If a linear model captures well the SOM dynamics in a

heterogeneous system, then either the underlying micro-scale dynamics are indeed linear, or the averaging of underlying nonlinear equations leads to linearity at macro-scale.

Conversely, we demonstrate that nonlinear kinetics at micro-scale do not remain the same when scaling up. The macro-scale dynamics retain a clear signature of nonlinearities at the micro-scale in the MFA term, but the second order terms could be even more important than the MFA. Thus, nonlinear kinetics might improve SOM predictions because microbial activity is accounted for (Wieder et al., 2013) (at the cost of increased uncertainty, Wieder et al. (2018)), but the question remains: which kinetic formulation should be used at the macro-scale that captures both microbial activity and spatial heterogeneities? We offer a framework to advance this area by using appropriately upscaled nonlinear kinetics including SOT at macro-scale. This upscaling framework can be extended to account for the role of other micro-scale interactions such as among substrates, microorganisms, and minerals, or even temporally varying connectivity due to water movement. These improvements, however, would come at the expense of increased number of nonlinear second order spatial moments.

To summarize, the proposed theoretical developments allow integration of spatial heterogeneity into decomposition kinetics. Assuming that the second order spatial moments are known, this integration can be achieved by using the equations listed in Table 2 instead of standard linear or nonlinear kinetic equations used in the current models (Wieder et al., 2018; Abramoff et al., 2018). However, the second order moments and their dynamics are not known in general, as discussed at the end of the following section.

4.4 Limitations of the upscaling approach

To illustrate the effects of spatial heterogeneities alone, we simulated idealized laboratory conditions in which the environmental conditions are constant so that the decomposition rate is not affected by soil moisture and temperature changes through time and space. Moreover, the simulated domain is small compared to an actual soil sample, but we regard the number of simulated grid cells (10^4) as representative of the range of variation occurring in larger, similarly idealized samples. In other studies, more complex micro-scale models based on nonlinear reactive and diffusive fluxes have been implemented (Monga et al., 2008; Nguyen-Ngoc et al., 2013; Monga et al., 2014); however, their spatial upscaling would require volume averaging of the coupled transport and reaction equations, making the problem mathematically intractable when aiming for analytical solutions (Whitaker, 1999; Valdés-Parada et al., 2009; Porter et al., 2011; Lugo-Méndez et al., 2015). The two pool micro-scale model with initial heterogeneous distributions of substrate and microorganisms as described in this study offers a simplified way of simulating reaction-diffusion systems. The two end-member cases of homogeneous and fully heterogeneous systems where grid cells are independent are representative of conditions in which diffusivities are high compared to reaction kinetics in the

former and negligible in the latter. In more realistic settings, conditions are likely to be intermediate between these two cases, as described by varying the value of the mass transfer coefficient α (Fig. 9).

Including C redistribution as a simple mass transfer process does not allow studying how soil structure affects macro-scale dynamics by creating and maintaining heterogeneous distributions of resources and oxygen, such as in aggregates (Keiluweit et al., 2017; Ebrahimi and Or, 2018). These patterns result from the interaction of transport and reaction processes that the proposed idealized models cannot capture.

The upscaling mechanism described in this work assumes that microbial mortality is first order in microbial C, so that this term remains structurally similar in the macroscopic Eqs. (13) and (14). A nonlinear mortality generalized by $T = k_B C_b^\beta$ (Georgiou et al., 2017) would create an additional term in the macro-scale equations. The mean microbial mortality can be calculated by inserting the nonlinear T into Eq. (16), resulting in $\bar{T} = k_B \bar{C}_b^\beta + \beta \bar{C}_b^{\beta-1} \sigma_{C_s}^2$, where $\sigma_{C_s}^2$ is the spatial variance of microbial C (for the biophysically heterogeneous system; i.e., k_B is spatially invariant). For $\beta = 1$, the first order mortality is recovered, (Eq. (22)); for $\beta \neq 1$, \bar{T} has an additional positive variance term that increases mortality at the macro-scale.

Finally, the upscaled macro-scale equations still require a closure scheme for integration; i.e., a set of equations linking the spatial moments to the mean state variables. With such a set of additional equations, the problem becomes mathematically 'closed', as the only remaining unknowns are the mean state variables. Examples of closure from other fields are mentioned in the introduction (e.g., Bergström et al. (2006)), but finding a robust closure scheme remains challenging and will be the subject of future work.

Moreover, our derivations are general, but how these closure equations are formulated and parameterized will likely depend on the scale transition under consideration - soil pore to core (as in this work), soil core to field, or even field to landscape. It is possible that a whole hierarchy of scale transitions is required to determine macro-scale equations suitable for regional or global-scale applications. Along similar lines, the number of terms in the Taylor expansion that should be retained at each level of this hierarchy remains an open question. It is also possible that the dynamics at the micro scale, in combination with C redistribution, lead to low values of higher order moments, because substrate consumption, mortality of the microorganisms, microbial mortality and transport contribute to smoothing spatial gradients.

25 5 Conclusions and perspective

Most carbon cycling models implicitly assume a spatially homogeneous distribution of SOM in different C pools and are based on the mean-field approximation of the rate of decomposition. However, assuming homogeneity is adequate only at the micro-scale in soils, due to the homogenizing effect of diffusion, which brings carbon sources and decomposers into direct contact

with each other at such scales. Therefore, the mean-field approximation is valid only at the micro-scale, creating a challenge when developing SOM models at macro-scale that also account for environmental heterogeneity. In this contribution, we used scale transition theory to link an idealized (but realistic) heterogeneous system and a homogeneous system by establishing an analytical expression for the macroscopic mean decomposition rate that accounts for the micro-scale heterogeneities. Unlike
5 the mean-field approximation adopted in most C cycling models, the upscaled governing equations we derived include second order spatial moments; i.e., spatial variances and/or covariances between micro-scale state variable and model parameters. The dynamical behavior of the second order terms drives the heterogeneous system away from the mean-field approximation. For a heterogeneous system, initially near steady state, micro-scale heterogeneities led to oscillations in the macro-scale respiration flux and higher SOM persistence in a fully heterogeneous system. For a heterogeneous system perturbed from its equilibrium,
10 the co-location of substrate and microorganisms increased macroscopic C fluxes compared to a case in which they were isolated.

In conclusion, this work provides a methodology to explicitly include micro-scale heterogeneity in soil C cycling models. Our upscaled kinetic equations could be used in lieu of current formulations, but additional equations describing the dynamics of spatial moments should be further developed to mathematically close the problem. The upscaled equations show that, (i)
15 heterogeneities alter the form of the carbon flux equations at the macro-scale and, as a result, (ii) co-location (respectively isolation) of microorganisms and their substrates promote (suppress) carbon fluxes in soils.

Code availability. The current version of codes used to construct the heterogeneous soil maps and to solve the mass balance equations in heterogeneous domains are publicly available from website: https://github.com/ArjunChakrawal/Heterogeneous_SOMDynamics under the MIT licence. The exact version of the model used to produce the results used in this paper is archived on Zenodo (Chakrawal, 2019), as
20 scripts to run the model and produce the plots for all the simulations presented in this paper (Chakrawal, 2019).

Data availability. The article does not use any relevant data.

Appendix A

A1 Derivation of the macro-scale rate of decomposition

Here we describe the derivation of the spatially averaged C flux for a generic microscopic C flux $F(C_s, C_b, k)$ using scale transition theory. As a first step, we calculate the multi-variate Taylor's series expansion of $F(C_s, C_b, k)$ around the spatial

5 average value of C_s, C_b and k ,

$$\begin{aligned}
 F(C_s, C_b, \mathbf{k}) &= F(\bar{C}_s, \bar{C}_b, \bar{\mathbf{k}}) + \frac{\partial F}{\partial C_s} \Big|_{\bar{C}_s, \bar{C}_b, \bar{\mathbf{k}}} (C_s - \bar{C}_s) + \frac{\partial F}{\partial C_b} \Big|_{\bar{C}_s, \bar{C}_b, \bar{\mathbf{k}}} (C_b - \bar{C}_b) + \\
 &\quad \sum_{i=1}^n \frac{\partial F}{\partial k_i} \Big|_{\bar{C}_s, \bar{C}_b, \bar{\mathbf{k}}} (k_i - \bar{k}_i) + \frac{1}{2} \frac{\partial^2 F}{\partial C_s^2} \Big|_{\bar{C}_s, \bar{C}_b, \bar{\mathbf{k}}} (C_s - \bar{C}_s)^2 + \frac{1}{2} \frac{\partial^2 F}{\partial C_b^2} \Big|_{\bar{C}_s, \bar{C}_b, \bar{\mathbf{k}}} (C_b - \bar{C}_b)^2 + \\
 &\quad \frac{1}{2} \sum_{i=1}^n \sum_{j=1}^n \frac{\partial^2 F}{\partial k_i \partial k_j} \Big|_{\bar{C}_s, \bar{C}_b, \bar{\mathbf{k}}} (k_i - \bar{k}_i)(k_j - \bar{k}_j) + \frac{\partial^2 F}{\partial C_s \partial C_b} \Big|_{\bar{C}_s, \bar{C}_b, \bar{\mathbf{k}}} (C_s - \bar{C}_s)(C_b - \bar{C}_b) + \\
 &\quad \sum_{i=1}^n \frac{\partial^2 F}{\partial k_i \partial C_s} \Big|_{\bar{C}_s, \bar{C}_b, \bar{\mathbf{k}}} (C_s - \bar{C}_s)(k_i - \bar{k}_i) + \sum_{i=1}^n \frac{\partial^2 F}{\partial k_i \partial C_b} \Big|_{\bar{C}_s, \bar{C}_b, \bar{\mathbf{k}}} (C_b - \bar{C}_b)(k_i - \bar{k}_i) + O(C_s^3 C_b^3 k_i^3), \quad (\text{A1})
 \end{aligned}$$

10 where $O(C_s^3, C_b^3, k_i^3)$ represents the higher order terms and the overbars denote the spatially averaged micro-scale quantities.

Second, the averaging operator given by Eq. (1) is applied in Eq. (A1). Truncating terms above the second order terms, Eq. (A1) becomes

$$\begin{aligned}
 \frac{1}{\int \int dx dy} \int \int F(C_s, C_b, \mathbf{k}) dx dy &= \\
 &\quad \frac{1}{\int \int dx dy} \left[F(\bar{C}_s, \bar{C}_b, \bar{\mathbf{k}}) + \frac{\partial F}{\partial C_s} \Big|_{\bar{C}_s, \bar{C}_b, \bar{\mathbf{k}}} (C_s - \bar{C}_s) + \frac{\partial F}{\partial C_b} \Big|_{\bar{C}_s, \bar{C}_b, \bar{\mathbf{k}}} (C_b - \bar{C}_b) + \right. \\
 15 &\quad \sum_{i=1}^n \frac{\partial F}{\partial k_i} \Big|_{\bar{C}_s, \bar{C}_b, \bar{\mathbf{k}}} (k_i - \bar{k}_i) + \frac{1}{2} \frac{\partial^2 F}{\partial C_s^2} \Big|_{\bar{C}_s, \bar{C}_b, \bar{\mathbf{k}}} (C_s - \bar{C}_s)^2 + \frac{1}{2} \frac{\partial^2 F}{\partial C_b^2} \Big|_{\bar{C}_s, \bar{C}_b, \bar{\mathbf{k}}} (C_b - \bar{C}_b)^2 + \\
 &\quad \frac{1}{2} \sum_{i=1}^n \sum_{j=1}^n \frac{\partial^2 F}{\partial k_i \partial k_j} \Big|_{\bar{C}_s, \bar{C}_b, \bar{\mathbf{k}}} (k_i - \bar{k}_i)(k_j - \bar{k}_j) + \frac{\partial^2 F}{\partial C_s \partial C_b} \Big|_{\bar{C}_s, \bar{C}_b, \bar{\mathbf{k}}} (C_s - \bar{C}_s)(C_b - \bar{C}_b) + \\
 &\quad \left. \sum_{i=1}^n \frac{\partial^2 F}{\partial k_i \partial C_s} \Big|_{\bar{C}_s, \bar{C}_b, \bar{\mathbf{k}}} (C_s - \bar{C}_s)(k_i - \bar{k}_i) + \sum_{i=1}^n \frac{\partial^2 F}{\partial k_i \partial C_b} \Big|_{\bar{C}_s, \bar{C}_b, \bar{\mathbf{k}}} (C_b - \bar{C}_b)(k_i - \bar{k}_i) \right]. \quad (\text{A2})
 \end{aligned}$$

In Eq. (A2), the first order partial derivatives (second, third and fourth term between the square brackets) disappear, because the partial derivatives evaluated at the mean state variables are constants that are multiplied by the expectation of the deviation

20 of a quantity, which is zero $\left(\frac{\partial F}{\partial \chi} \Big|_{\bar{\chi}} \int \int (\chi - \bar{\chi}) dx dy = 0 \right)$, where χ is C_s, C_b or k .

Finally, after applying the averaging operator, deviations multiplying the second order partial derivatives become spatial variances and covariances. As a result, the macro-scale C flux $\overline{F}(C_s, C_b, \mathbf{k})$ is obtained

$$\begin{aligned} \overline{F}(C_s, C_b, \mathbf{k}) = & F(\overline{C}_s, \overline{C}_b, \overline{\mathbf{k}}) + \frac{1}{2} \frac{\partial^2 F}{\partial C_s^2} \Big|_{\overline{C}_s, \overline{C}_b, \overline{\mathbf{k}}} \sigma_{C_s}^2 + \frac{1}{2} \frac{\partial^2 F}{\partial C_b^2} \Big|_{\overline{C}_s, \overline{C}_b, \overline{\mathbf{k}}} \sigma_{C_b}^2 + \sum_{i=1}^n \sum_{j=1}^n \frac{\partial^2 F}{\partial k_i \partial k_j} \Big|_{\overline{C}_s, \overline{C}_b, \overline{\mathbf{k}}} \overline{k'_i k'_j} \\ & \frac{\partial^2 F}{\partial C_s \partial C_b} \Big|_{\overline{C}_s, \overline{C}_b, \overline{\mathbf{k}}} \overline{C'_s C'_b} + \sum_{i=1}^n \frac{\partial^2 F}{\partial k_i \partial C_s} \Big|_{\overline{C}_s, \overline{C}_b, \overline{\mathbf{k}}} \overline{k'_i C'_s} + \sum_{i=1}^n \frac{\partial^2 F}{\partial k_i \partial C_b} \Big|_{\overline{C}_s, \overline{C}_b, \overline{\mathbf{k}}} \overline{k'_i C'_b}, \end{aligned} \quad (\text{A3})$$

5 Equation (A3) can be used to obtain the macro-scale C flux given the decomposition function D at micro-scale. Explicit solutions for the multiplicative kinetics are reported in the main text (Eq. (18), (20), and (21)).

For illustration, here we report the derivation of the spatially averaged rate of decomposition for Michaelis-Menten (MM) kinetics. The micro-scale rate of decomposition for MM kinetics is given by

$$F = \frac{k_{MM} C_s C_b}{K_{MM} + C_s} \quad (\text{A4})$$

10 where both the parameters k_{MM} and K_{MM} and the state variables C_s and C_b are considered spatially variable quantities. Inserting Eq. (A4) into Eq. (16) gives the macro-scale rate of decomposition

$$\begin{aligned} \overline{F}(C_s, C_b, [k_{MM}, K_{MM}]) = & F(\overline{C}_s, \overline{C}_b, \overline{k}_{MM}, \overline{K}_{MM}) + \frac{1}{2} \frac{\partial^2 F}{\partial C_s^2} \Big|_{\overline{C}_s, \overline{C}_b, \overline{k}_{MM}, \overline{K}_{MM}} \sigma_{C_s}^2 + \frac{1}{2} \frac{\partial^2 F}{\partial k_{MM}^2} \Big|_{\overline{C}_s, \overline{C}_b, \overline{k}_{MM}, \overline{K}_{MM}} \sigma_{k_{MM}}^2 + \\ & \frac{1}{2} \frac{\partial^2 F}{\partial k_{MM}^2} \Big|_{\overline{C}_s, \overline{C}_b, \overline{k}_{MM}, \overline{K}_{MM}} \sigma_{k_{MM}}^2 + \frac{\partial^2 F}{\partial k_{MM} \partial K_{MM}} \Big|_{\overline{C}_s, \overline{C}_b, \overline{k}_{MM}, \overline{K}_{MM}} \overline{k'_{MM} K'_{MM}} + \\ 15 & \frac{\partial^2 F}{\partial C_s \partial C_b} \Big|_{\overline{C}_s, \overline{C}_b, \overline{k}_{MM}, \overline{K}_{MM}} \overline{C'_s C'_b} + \frac{\partial^2 F}{\partial k_{MM} \partial C_s} \Big|_{\overline{C}_s, \overline{C}_b, \overline{k}_{MM}, \overline{K}_{MM}} \overline{C'_s k'_{MM}} + \\ & \frac{\partial^2 F}{\partial k_{MM} \partial C_b} \Big|_{\overline{C}_s, \overline{C}_b, \overline{k}_{MM}, \overline{K}_{MM}} \overline{C'_b k'_{MM}} + \frac{\partial^2 F}{\partial K_{MM} \partial C_s} \Big|_{\overline{C}_s, \overline{C}_b, \overline{k}_{MM}, \overline{K}_{MM}} \overline{C'_s K'_{MM}} + \\ & \frac{\partial^2 F}{\partial K_{MM} \partial C_b} \Big|_{\overline{C}_s, \overline{C}_b, \overline{k}_{MM}, \overline{K}_{MM}} \overline{C'_b K'_{MM}}. \end{aligned} \quad (\text{A5})$$

The partial derivative of F with respect to k_{MM} is zero because F is a linear function of k_{MM} . Now, for biophysical heterogeneous and biochemical homogeneous system, covariances and variances related to parameters are zeros so that we are left

with

$$\bar{F}(C_s, C_b, [k_{MM}, K_{MM}]) = F(\bar{C}_s, \bar{C}_b, \bar{k}_{MM}, \bar{K}_{MM}) + \frac{1}{2} \frac{\partial^2 F}{\partial C_s^2} \Big|_{\bar{C}_s, \bar{C}_b, \bar{k}_{MM}, \bar{K}_{MM}} \sigma_{C_s}^2 + \frac{\partial^2 F}{\partial C_s \partial C_b} \Big|_{\bar{C}_s, \bar{C}_b, \bar{k}_{MM}, \bar{K}_{MM}} \overline{C'_s C'_b}. \quad (\text{A6})$$

Calculating the derivatives gives

$$\bar{F}(C_s, C_b, [k_{MM}, K_{MM}]) = \frac{k_{MM} \bar{C}_s \bar{C}_b}{K_{MM} + \bar{C}_s} + \frac{1}{2} \left[\frac{-2k_{MM} K_{MM} \bar{C}_b}{(K_{MM} + \bar{C}_s)^3} \right] \sigma_{C_s}^2 + \left[\frac{k_{MM} K_{MM}}{(\bar{C}_s + K_{MM})^2} \right] \overline{C'_s C'_b}. \quad (\text{A7})$$

- 5 For biophysical homogeneous and biochemical heterogeneous system, covariances and variances of state variables (C_s and C_b) are zeros so that we are left with

$$\begin{aligned} \bar{F}(C_s, C_b, [k_{MM}, K_{MM}]) = & F(\bar{C}_s, \bar{C}_b, \bar{k}_{MM}, \bar{K}_{MM}) + \frac{1}{2} \frac{\partial^2 F}{\partial k_{MM}^2} \Big|_{\bar{C}_s, \bar{C}_b, \bar{k}_{MM}, \bar{K}_{MM}} \sigma_{k_{MM}}^2 + \\ & \frac{\partial^2 F}{\partial k_{MM} \partial K_{MM}} \Big|_{\bar{C}_s, \bar{C}_b, \bar{k}_{MM}, \bar{K}_{MM}} \overline{k'_{MM} K'_{MM}} + \frac{\partial^2 F}{\partial k_{MM} \partial C_s} \Big|_{\bar{C}_s, \bar{C}_b, \bar{k}_{MM}, \bar{K}_{MM}} \overline{C'_s k'_{MM}} + \\ & \frac{\partial^2 F}{\partial k_{MM} \partial C_b} \Big|_{\bar{C}_s, \bar{C}_b, \bar{k}_{MM}, \bar{K}_{MM}} \overline{C'_b k'_{MM}} + \frac{\partial^2 F}{\partial K_{MM} \partial C_s} \Big|_{\bar{C}_s, \bar{C}_b, \bar{k}_{MM}, \bar{K}_{MM}} \overline{C'_s K'_{MM}} + \\ & \frac{\partial^2 F}{\partial K_{MM} \partial C_b} \Big|_{\bar{C}_s, \bar{C}_b, \bar{k}_{MM}, \bar{K}_{MM}} \overline{C'_b K'_{MM}}. \end{aligned} \quad (\text{A8})$$

10

For a completely heterogeneous system with biophysical and biochemical heterogeneity, the mean rate of decomposition at macro-scale is given by Eq. (A9).

$$\begin{aligned}
\bar{F}(C_s, C_b, [k_{MM}, K_{MM}]) = & \\
& F(\bar{C}_s, \bar{C}_b, \bar{k}_{MM}, \bar{K}_{MM}) + \frac{1}{2} \frac{\partial^2 F}{\partial C_s^2} \Big|_{\bar{C}_s, \bar{C}_b, \bar{k}_{MM}, \bar{K}_{MM}} \sigma_{C_s}^2 + \\
& \frac{1}{2} \frac{\partial^2 F}{\partial K_{MM}^2} \Big|_{\bar{C}_s, \bar{C}_b, \bar{k}_{MM}, \bar{K}_{MM}} \sigma_{K_{MM}}^2 + \frac{\partial^2 F}{\partial k_{MM} \partial K_{MM}} \Big|_{\bar{C}_s, \bar{C}_b, \bar{k}_{MM}, \bar{K}_{MM}} \overline{k'_{MM} K'_{MM}} + \\
& \frac{\partial^2 F}{\partial C_s \partial C_b} \Big|_{\bar{C}_s, \bar{C}_b, \bar{k}_{MM}, \bar{K}_{MM}} \overline{C'_s C'_b} + \frac{\partial^2 F}{\partial k_{MM} \partial C_s} \Big|_{\bar{C}_s, \bar{C}_b, \bar{k}_{MM}, \bar{K}_{MM}} \overline{C'_s k'_{MM}} + \\
& \frac{\partial^2 F}{\partial k_{MM} \partial C_b} \Big|_{\bar{C}_s, \bar{C}_b, \bar{k}_{MM}, \bar{K}_{MM}} \overline{C'_b k'_{MM}} + \frac{\partial^2 F}{\partial K_{MM} \partial C_s} \Big|_{\bar{C}_s, \bar{C}_b, \bar{k}_{MM}, \bar{K}_{MM}} \overline{C'_s K'_{MM}} + \\
& \frac{\partial^2 F}{\partial K_{MM} \partial C_b} \Big|_{\bar{C}_s, \bar{C}_b, \bar{k}_{MM}, \bar{K}_{MM}} \overline{C'_b K'_{MM}}. \tag{A9}
\end{aligned}$$

Similar to MM kinetics, the mean rate of decomposition for IMM kinetics can also be calculated as,

$$\begin{aligned}
10 \quad \bar{F}(C_s, C_b, [k_{IMM}, K_{IMM}]) = & \\
& F(\bar{C}_s, \bar{C}_b, \bar{k}_{IMM}, \bar{K}_{IMM}) + \frac{1}{2} \frac{\partial^2 F}{\partial C_s^2} \Big|_{\bar{C}_s, \bar{C}_b, \bar{k}_{IMM}, \bar{K}_{IMM}} \sigma_{C_b}^2 + \\
& \frac{1}{2} \frac{\partial^2 F}{\partial K_{IMM}^2} \Big|_{\bar{C}_s, \bar{C}_b, \bar{k}_{IMM}, \bar{K}_{IMM}} \sigma_{K_{IMM}}^2 + \frac{\partial^2 F}{\partial k_{IMM} \partial K_{IMM}} \Big|_{\bar{C}_s, \bar{C}_b, \bar{k}_{IMM}, \bar{K}_{IMM}} \overline{k'_{IMM} K'_{IMM}} + \\
& \frac{\partial^2 F}{\partial C_s \partial C_b} \Big|_{\bar{C}_s, \bar{C}_b, \bar{k}_{IMM}, \bar{K}_{IMM}} \overline{C'_s C'_b} + \frac{\partial^2 F}{\partial k_{IMM} \partial C_s} \Big|_{\bar{C}_s, \bar{C}_b, \bar{k}_{IMM}, \bar{K}_{IMM}} \overline{C'_s k'_{IMM}} + \\
& \frac{\partial^2 F}{\partial k_{IMM} \partial C_b} \Big|_{\bar{C}_s, \bar{C}_b, \bar{k}_{IMM}, \bar{K}_{IMM}} \overline{C'_b k'_{IMM}} + \frac{\partial^2 F}{\partial K_{IMM} \partial C_s} \Big|_{\bar{C}_s, \bar{C}_b, \bar{k}_{IMM}, \bar{K}_{IMM}} \overline{C'_s K'_{IMM}} + \\
15 \quad & \frac{\partial^2 F}{\partial K_{IMM} \partial C_b} \Big|_{\bar{C}_s, \bar{C}_b, \bar{k}_{IMM}, \bar{K}_{IMM}} \overline{C'_b K'_{IMM}}. \tag{A10}
\end{aligned}$$

A2 Initial 2D random fields of substrate C and microbial C

The heterogeneous field of microbial C was created using a random field generator that provides 100×100 spatially correlated random numbers between -1 and 1 (Lennon, 2000). These values were then re-scaled by an appropriate mean and standard deviation of microbial C. To simulate the dead zones in the heterogeneous system, some grid cells were forced to have no microbial C (the obtained field is denoted $\mathbf{y}_{i,j}$). Moreover, to allow comparison among simulations, the microbial C field was

re-normalized to have a specified value of total initial microbial C,

$$C_{b,i,j} = \frac{y_{i,j}}{\sum_{i,j} y_{i,j}} C_{b,total} \text{ (fg)} \quad (\text{A11})$$

It is assumed that the $C_{b,total}$ is equal to 1% of the total amount of substrate in the domain (Witter, 1996), which is in turn calculated as $C_{s,total} = \bar{C}_{s,0} \times N_x \times N_y$ where $\bar{C}_{s,0}$ is the initial mean substrate C in a single grid cell (fg). The amount of substrate C in any grid cell is limited by the maximum amount of C that the cell can accommodate, according to the density of organic matter (ρ_{SOM}), and assuming that 50% of organic matter on a mass basis is composed of organic C. The maximum amount of substrate C that one cell can contain is thus given by

$$C_{max} = 0.5\rho_{SOM} \text{ cell}_{volume} \text{ (fg)} \quad (\text{A12})$$

where cell_{volume} is the volume of a grid cell. The value of $\bar{C}_{s,0}$ was chosen so that the maximum C amount at a micro-site does not exceed C_{max} . To summarize, the obtained spatially heterogeneous random fields of microbial C and substrate C satisfy the following constraints: i) the total amount of organic C is set, ii) the total amount of microbial C is 1% of total organic C, iii) the maximum amount of C in a cell is set (Eq. (A12)), and iv) some grid cells have no microbial biomass.

A3 Steady state substrate C for the multiplicative kinetics in the fully heterogeneous systems

The substrate C at steady state for all decomposition kinetics is given in Table 1, and is restated here for multiplicative kinetics only,

$$C_s^* = \frac{k_B}{Yk_M}, \quad (\text{A13})$$

where * represents steady state conditions. Eq. (A13) show that the steady state substrate C depends only on the kinetic parameters and microbial C-use efficiency. Thus, if the kinetic parameters are spatially variable (i.e., fully heterogeneous system) then C_s^* is also spatially variable and different from the steady state values of biophysically heterogeneous or homogeneous systems. Knowing the probability distributions of the kinetic parameters, the mean steady state substrate C in the fully heterogeneous system can be calculated as the mean value of C_s^* .

The mean value of a generic function, $g(x)$ is given by $\overline{g(x)} = \int_{-\infty}^{\infty} g(x)f_X(x)dx$, where $f_X(x)$ is the probability density function of x . Accordingly, the mean value of C_s^* is given by,

$$\overline{C_s^*} = \int_a^b \frac{k_B}{Yk_M} f(k_M)dk_M \quad (\text{A14})$$

where $f(k_M)$ is the probability density function of k_M . As in Forney and Rothman (2012), we can assume that the kinetic constant k_M follows a log-uniform distribution $f(k_M) = \frac{1}{(b-a)k_M \ln 10}$, with mean $\frac{10^a - 10^b}{(b-a) \ln(10)}$ where a and b are the parameters of log-uniform distribution. With this distribution the mean C_s^* becomes,

$$\overline{C_s^*} = \frac{k_B (10^{-a} - 10^{-b})}{Y(b-a) \ln(10)} \quad (\text{A15})$$

Equation (A15) shows that $\overline{C_s^*}$ in the heterogeneous system deviates from the value attained in a homogeneous system because in general k_M differs from $\frac{(b-a) \ln(10)}{10^{-a} - 10^{-b}}$. Similar derivations can be made for the other formulations of decomposition kinetics.

A4 Sensitivity of simulated fluctuations to changes in k_M in scenario 1

We performed two sensitivity analyses in which we altered the kinetic constant parameter for the multiplicative decomposition model k_M : 1) decreasing k_M in the system with biophysical heterogeneity–positively correlated C_s and C_b (Fig. A1) and 2) increasing the heterogeneity of k_M (by increasing its standard deviation) in the full heterogeneity case (Fig. A2). From Fig. A1, it is clear that decreasing the rate constant increases the amplitude and wavelength of the oscillations. As shown in Fig. A2, increasing the heterogeneity of the rate constant increases the amount of undecomposed substrate C compared to a lower degree of heterogeneity (Fig. 4). This pattern can be explained using the analytical expression of the steady state substrate C (see Eq. (A15) in Appendix A3). For the increased heterogeneity case shown in Fig. 4, we used values of a and b as listed in Table A3 for biochemical heterogeneity 1 and multiplicative kinetics, where a and b have the same meaning as in Eq. (A15). The analytical expression for the steady state, evaluated with these values of a and b , results in exactly the same steady state of substrate C as simulated by the distributed model (i.e., 15 mgC/gSoil).

These fluctuations are similar to those noted in earlier papers using spatially lumped models (Manzoni and Porporato, 2007; Sierra and Muller, 2015). These papers showed that the occurrence and amplitude of the fluctuations depend on the kinetic parameter values, as is the case here.

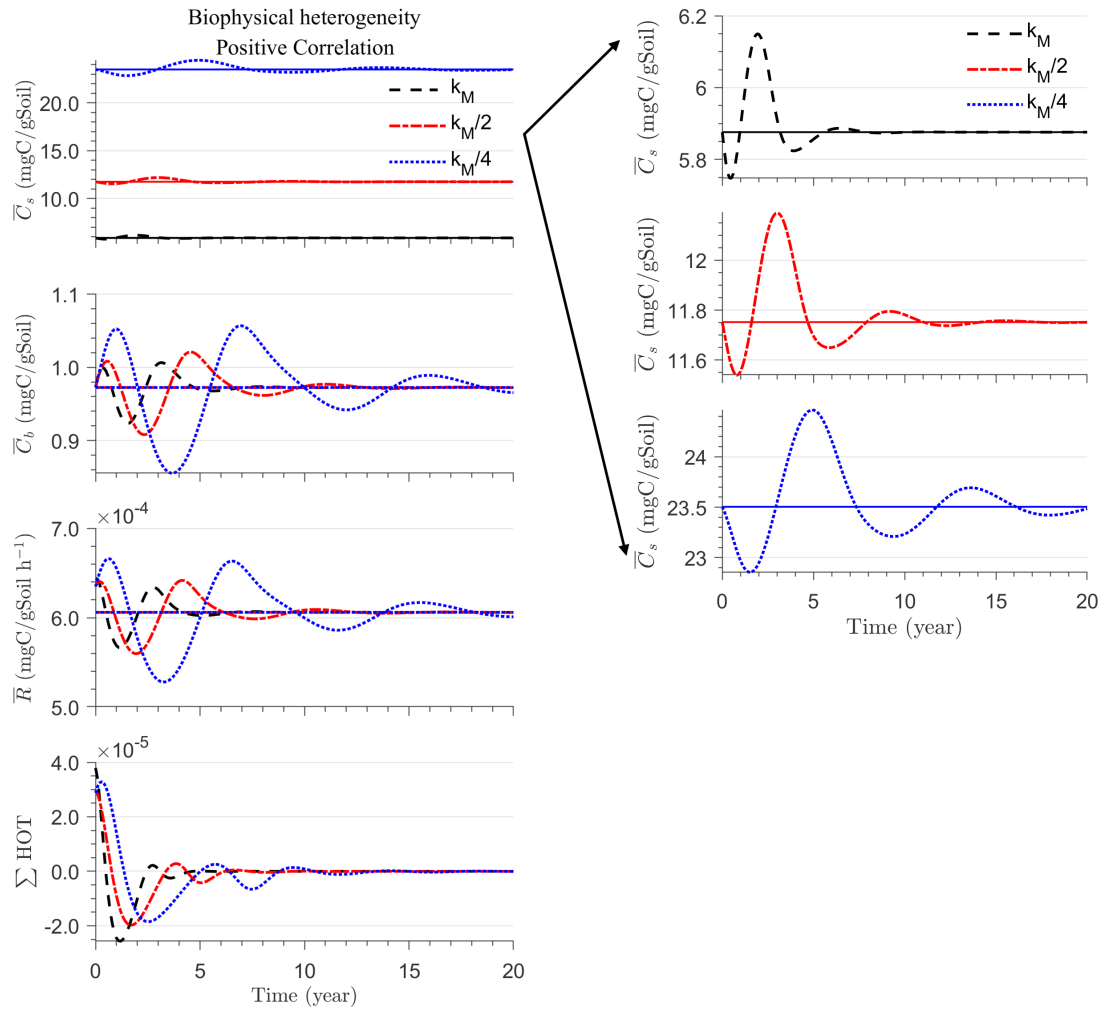


Figure A1. (a) mean substrate C (\bar{C}_s), (b) mean microbial C (\bar{C}_b), (c) mean respiration rate (\bar{R}), and (d) sum of second and third order terms ($\sum HOT$) are shown as a function of time, for positively correlated initial spatial heterogeneity of C_s and C_b . This figure is similar to Fig. 4, left column (initial substrate is distributed randomly around the steady state). Varying levels of the rate constant k_M are shown (as indicated by different line styles and colors; the base case is the same as in Fig. 4). Panels on the right are enlarged views of the time trajectories of \bar{C}_s .

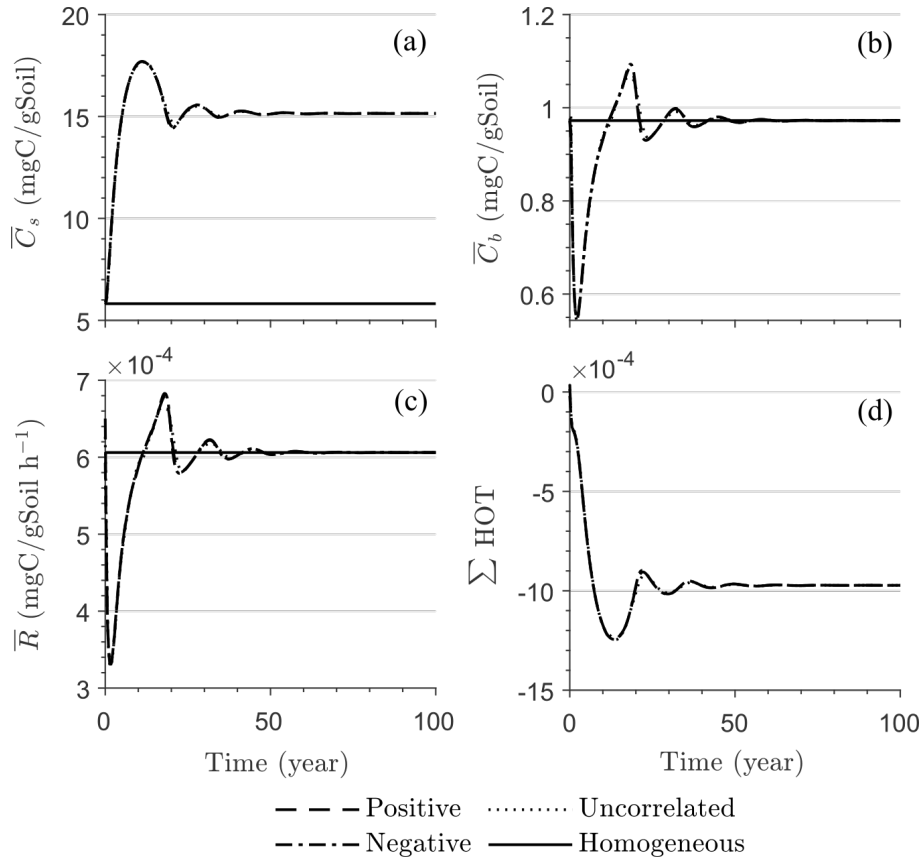


Figure A2. (a) mean substrate C (\bar{C}_s), (b) mean microbial C (\bar{C}_b), (c) mean respiration rate (\bar{R}), and (d) sum of second and third order terms ($\sum HOT$) are shown as a function of time, for different scenarios of initial spatial heterogeneity. This figure is similar to Fig. 4 for the full heterogeneity case, but with increased heterogeneity of the rate constant (k_M).

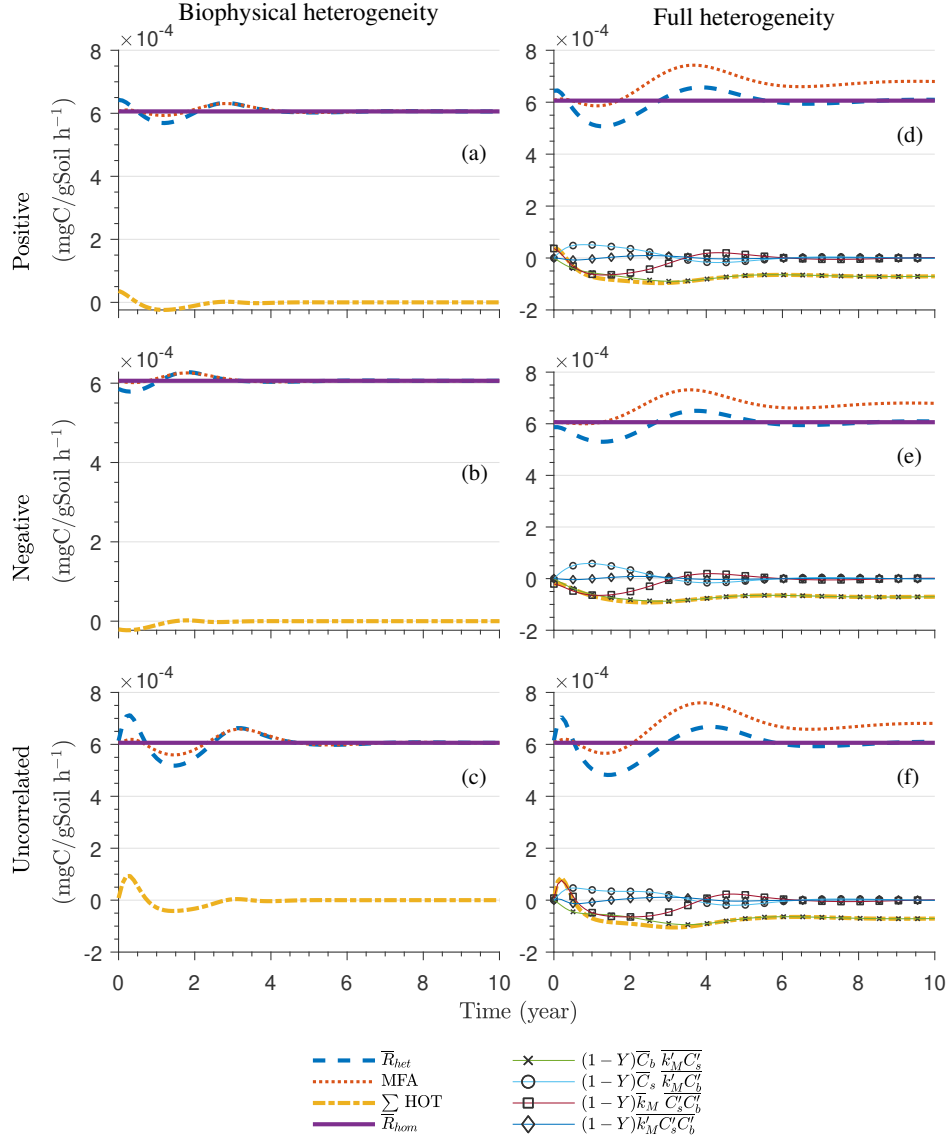


Figure A3. Scenario 1 (steady state simulation): temporal evolution of mean respiration rate in the heterogeneous system (\bar{R}_{het} , including the mean-field approximation (MFA) and second order terms), and the respiration rate in the homogeneous system (\bar{R}_{hom}), for multiplicative kinetics and for (a–c) the biophysical and (d–f) the fully heterogeneous system with (a–d) positively and (b–e) negatively correlated, or (c–f) uncorrelated initial substrate and microbial C.

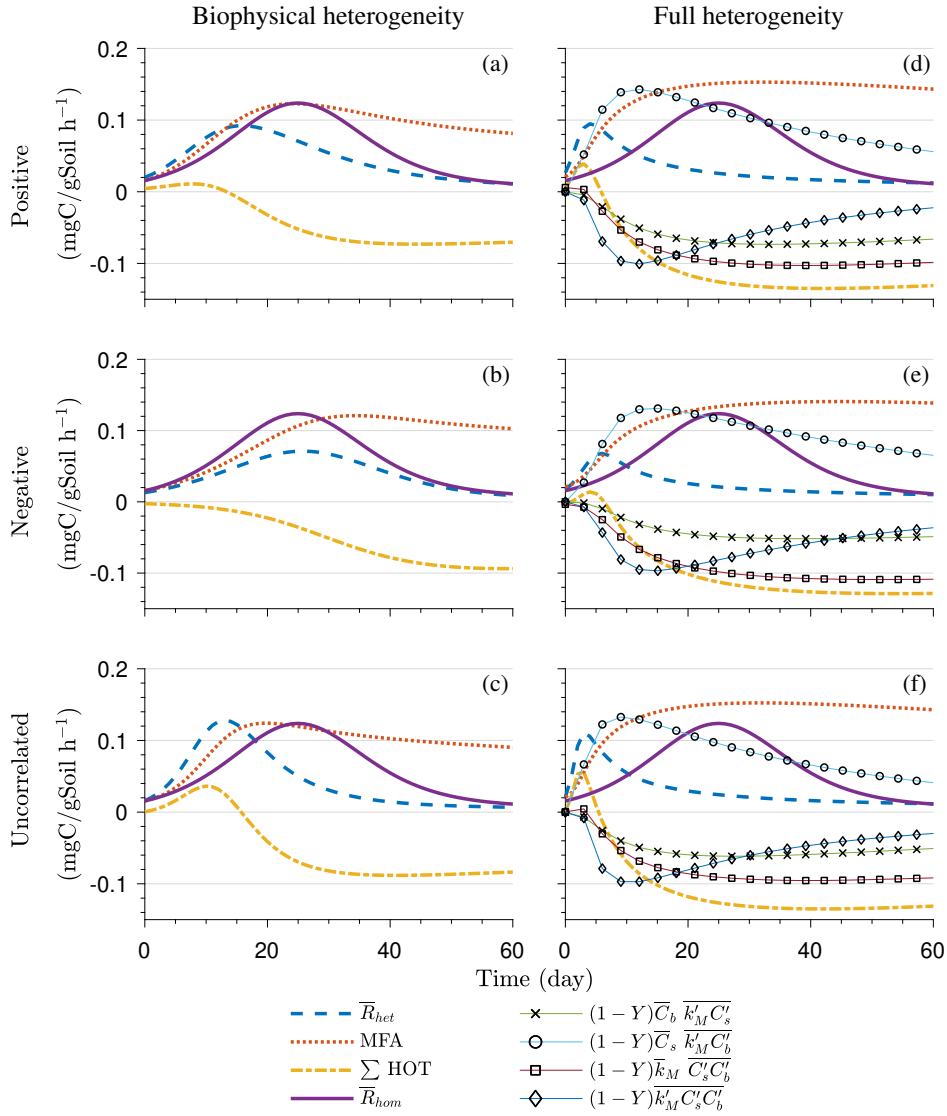


Figure A4. Scenario 2 (HS simulation with multiplicative kinetics): temporal evolution of mean respiration rate in the heterogeneous system (\bar{R}_{het}), which includes the mean-field approximation (MFA) and second order terms, and the respiration rate in the homogeneous system (\bar{R}_{hom}), for (a–c) the biophysically and (d–f) the fully heterogeneous system with positive (a–b), negative (c–d) and un-correlated (e–f) substrate and microbial C, for multiplicative kinetics.

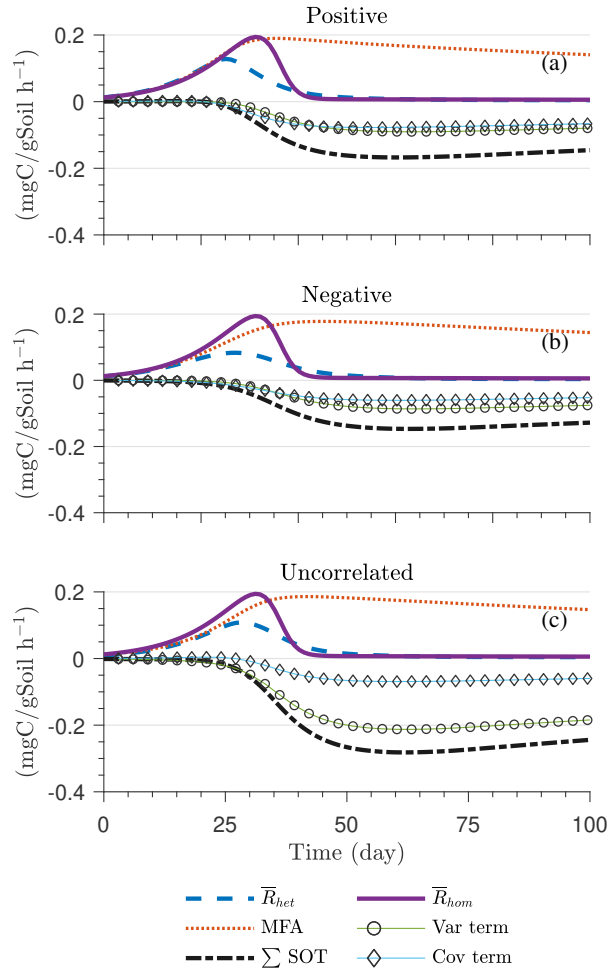


Figure A5. Scenario 2 (HS with Michaelis-Menten kinetics): temporal evolution of mean respiration rate in the biophysically heterogeneous system (\bar{R}_{het} , including the mean-field approximation (MFA) and second order terms), and the respiration rate in the homogeneous system (\bar{R}_{hom}), for (a) positively and (b) negatively correlated, or (c) uncorrelated substrate and microbial C.

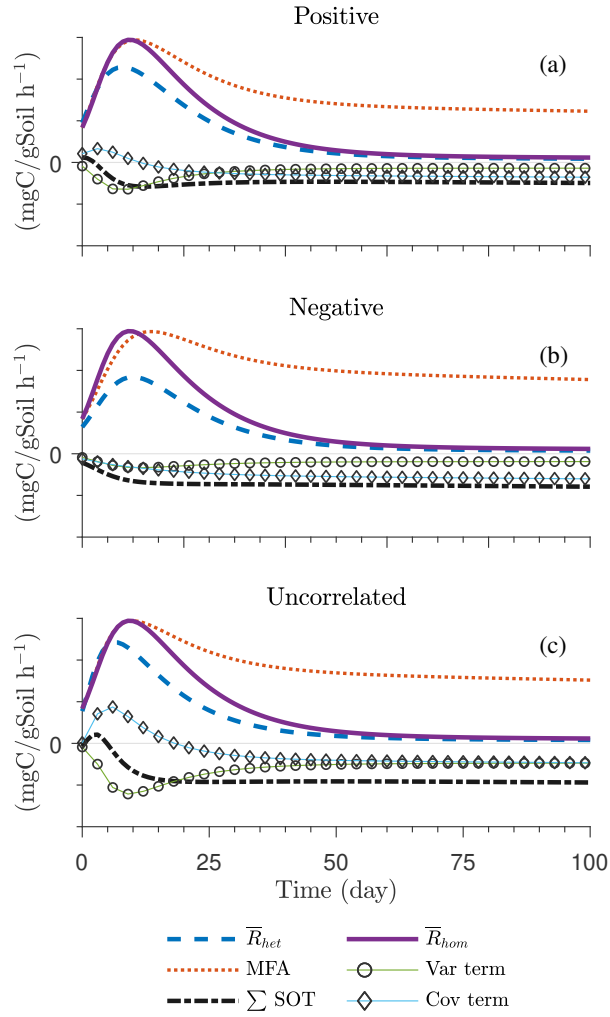


Figure A6. Scenario 2 (HS with inverse Michaelis-Menten kinetics): temporal evolution of mean respiration rate in the biophysically heterogeneous system (\bar{R}_{het} , including the mean-field approximation (MFA) and second order terms), and the respiration rate in the homogeneous system (\bar{R}_{hom}), for (a) positively and (b) negatively correlated, or (c) uncorrelated substrate and microbial C.

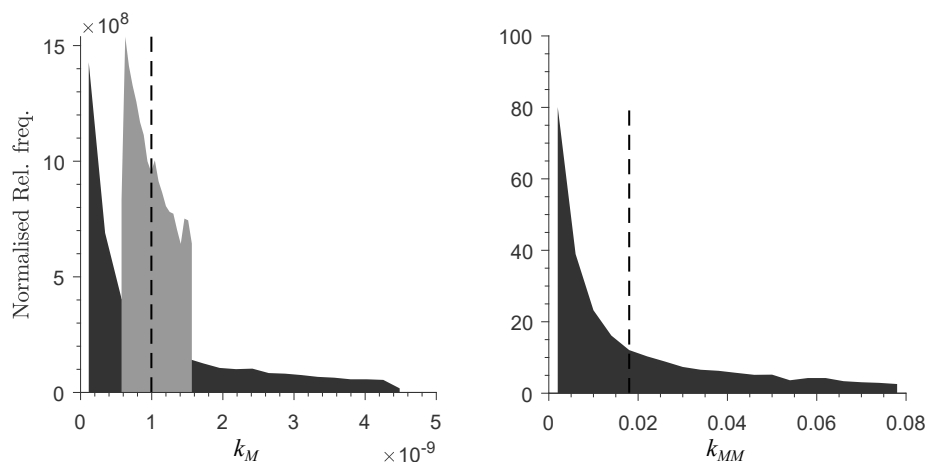


Figure A7. Distribution of the decomposition rate constant for different degrees of biochemical heterogeneity, and for (a) multiplicative and (b) Michaelis-Menten kinetics. Black and grey shadings represent higher and lower degree of biochemical heterogeneity, respectively, and the dashed line represents the mean rate constant for the homogeneous system. The half saturation constant K_{MM} is uniformly distributed, not shown in figure.

Table A1. List of parameters. Values in brackets correspond to the units reported in brackets.

Parameter	Value	Unit	Description
I	6.06×10^{-4}	$\text{mgCg}^{-1}\text{soil h}^{-1}$	Rate of input of external carbon
K_{MM}	5156250 (25)	fgC/grid cell $(\text{mgCg}^{-1}\text{soil})$	Half saturation constant (MM)
k_{MM}	0.018	h^{-1}	Decomposition rate constant for the MM kinetics
K_{IMM}	2×10^6 (9.69)	fgC/grid cell $(\text{mgCg}^{-1}\text{soil})$	Half saturation constant (IMM)
k_{IMM}	0.0045	h^{-1}	Decomposition rate constant for the IMM kinetics
k_M	7.45×10^{-10} (1.53×10^{-4})	$\text{h}^{-1} (\text{fgC/grid cell})^{-1}$ $(\text{h}^{-1} (\text{mgCg}^{-1}\text{soil})^{-1})$	Decomposition rate constant for the Multiplicative kinetics
k_B	0.00028	h^{-1}	Decomposition rate constant for the MM kinetics
Y	0.31	-	microbial C-use efficiency
ρ_{BD}	1.65	g/cm^3	Soil bulk density
ρ_{OM}	1.1	g/cm^3	Organic matter density

Table A2. Initial mean substrate and microbial C in scenarios SS and HS, expressed in both fgC/grid cell and $\text{mgCg}^{-1}\text{soil}$ (values in brackets).

Scenario	Initial \bar{C}_s	Initial \bar{C}_b
	$\text{fgC/grid cell}(\text{mgCg}^{-1}\text{soil})$	
Steady state simulation (SS)	1.212×10^5 (5.9)	2.005×10^5 (0.9725)
High substrate simulation (HS)	2.5×10^7 (121.21)	2.5×10^5 (1.21)

Table A3. Probability distributions of the parameters for the multiplicative, MM, and IMM kinetics models. Values in brackets indicate the minimum and maximum parameter values.

		Biochemical heterogeneity 1	Biochemical heterogeneity 2
Multiplicative	k_M	$\log_{10}\text{Uniform}(-10.1, -8.56)$	$\log_{10}\text{Uniform}(-9.4, -8.9)$
	$(\text{h}^{-1}) (\text{fgC/grid cell})^{-1}$		
MM	k_{MM} (h^{-1})	$\log_{10}\text{Uniform}(-1.098, -3)$	
	K_{MM} (fgC/grid cell)	$\text{Uniform}(0.25, 49.75)$	
IMM	k_{IMM} (h^{-1})	$k_{MM}/4$	
	K_{IMM} (fgC/grid cell)	$\text{Uniform}(1, 18.4)$	

Author contributions. All authors conceived the initial conceptualization. Arjun Chakrawal and Stefano Manzoni developed the theoretical formalism and performed the analytic calculations. Arjun Chakrawal performed the numerical simulations and led the writing of the manuscript. All authors discussed the results, provided critical feedback, and revised the manuscript.

Acknowledgements. This research was supported by the Swedish Research Councils Vetenskapsrådet (grant 2016-04146) and Formas (grant 5 2015-468). We thank Thomas Wutzler, Ali Ebrahimi, and an anonymous reviewer for their insightful comments.

References

- Abramoff, R., Xu, X., Hartman, M., O'Brien, S., Feng, W., Davidson, E., Finzi, A., Moorhead, D., Schimel, J., Torn, M., et al.: The Millennial model: in search of measurable pools and transformations for modeling soil carbon in the new century, *Biogeochemistry*, 137, 51–71, 2018.
- Albertson, J. D. and Montaldo, N.: Temporal dynamics of soil moisture variability: 1. Theoretical basis, *Water Resources Research*, 39, 1–14, <https://doi.org/10.1029/2002WR001616>, 2003.
- Aleklett, K., Kiers, E. T., Ohlsson, P., Shimizu, T. S., Caldas, V. E., and Hammer, E. C.: Build Your Own Soil: Exploring Microfluidics to Create Microbial Habitat Structures, *The ISME Journal*, 12, 312–319, <https://doi.org/10.1038/ismej.2017.184>, 2018.
- Allison, S. D.: Cheaters, diffusion and nutrients constrain decomposition by microbial enzymes in spatially structured environments, *Ecology Letters*, 8, 626–635, <https://doi.org/10.1111/j.1461-0248.2005.00756.x>, 2005.
- 10 Allison, S. D.: A trait-based approach for modelling microbial litter decomposition, <https://doi.org/10.1111/j.1461-0248.2012.01807.x>, 2012.
- Barraquand, F. and Murrell, D. J.: Scaling up predator-prey dynamics using spatial moment equations, *Methods in Ecology and Evolution*, 4, 276–289, <https://doi.org/10.1111/2041-210X.12014>, 2013.
- Bergström, U., Englund, G., and Leonardsson, K.: Plugging space into predator-prey models: an empirical approach., *The American naturalist*, 167, 246–259, <https://doi.org/10.1086/499372>, 2006.
- 15 Bouckaert, L., Sleutel, S., Van Loo, D., Brabant, L., Cnudde, V., Van Hoorebeke, L., and De Neve, S.: Carbon mineralisation and pore size classes in undisturbed soil cores, *Soil Research*, 51, 14–22, <https://doi.org/10.1071/SR12116>, 2013.
- Chakrawal, A.: Dynamic upscaling of decomposition kinetics for carbon cycling models: Heterogeneous_SOMDynamics-v2.0, <https://doi.org/10.5281/zenodo.3576613>, 2019.
- Chesson, P.: Making sense of spatial models in ecology, *Modeling spatiotemporal dynamics in ecology*, pp. 151–166, 1998.
- 20 Dagan, G.: Theory of solute transport by groundwater, *Annual review of fluid mechanics*, 19, 183–213, <https://doi.org/10.1146/annurev.fl.19.010187.001151>, 1987.
- Dentz, M., Le Borgne, T., Englert, A., and Bijeljic, B.: Mixing, spreading and reaction in heterogeneous media: A brief review, *Journal of Contaminant Hydrology*, 120-121, 1–17, <https://doi.org/10.1016/j.jconhyd.2010.05.002>, 2011.
- Don, A., Rödenbeck, C., and Gleixner, G.: Unexpected control of soil carbon turnover by soil carbon concentration, *Environmental Chemistry Letters*, 11, 407–413, 2013.
- 25 Dungait, J. A., Hopkins, D. W., Gregory, A. S., and Whitmore, A. P.: Soil organic matter turnover is governed by accessibility not recalcitrance, *Global Change Biology*, 18, 1781–1796, <https://doi.org/10.1111/j.1365-2486.2012.02665.x>, 2012.
- Ebrahimi, A. and Or, D.: Microbial community dynamics in soil aggregates shape biogeochemical gas fluxes from soil profiles - upscaling an aggregate biophysical model, *Global change biology*, 22, 3141–3156, <https://doi.org/10.1111/gcb.13345>, 2016.

- Ekschmitt, K., Kandeler, E., Poll, C., Brune, A., Buscot, F., Friedrich, M., Gleixner, G., Hartmann, A., Kästner, M., Marhan, S., Miltner, A., Scheu, S., and Wolters, V.: Soil-carbon preservation through habitat constraints and biological limitations on decomposer activity, <https://doi.org/10.1002/jpln.200700051>, 2008.
- Englund, G. and Leonardsson, K.: Scaling up the functional response for spatially heterogeneous systems, *Ecology Letters*, 11, 440–449, <https://doi.org/10.1111/j.1461-0248.2008.01159.x>, 2008.
- 5 Falconer, R. E., Battaia, G., Schmidt, S., Baveye, P., Chenu, C., and Otten, W.: Microscale Heterogeneity Explains Experimental Variability and Non-Linearity in Soil Organic Matter Mineralisation, *PLOS ONE*, 10, e0123774, <https://doi.org/10.1371/journal.pone.0123774>, 2015.
- Fatichi, S., Katul, G. G., Ivanov, V. Y., Pappas, C., Paschalis, A., Consolo, A., Kim, J., and Burlando, P.: Abiotic and biotic controls of soil moisture spatiotemporal variability and the occurrence of hysteresis, *Water Resources Research*, 51, 3505–3524, <https://doi.org/10.1002/2014WR016102>, 2015.
- 10 Forney, D. C. and Rothman, D. H.: Common structure in the heterogeneity of plant-matter decay, *Journal of the Royal Society Interface*, 9, 2255–2267, <https://doi.org/10.1098/rsif.2012.0122>, 2012.
- Fraser, F. C., Todman, L. C., Corstanje, R., Deeks, L. K., Harris, J. A., Pawlett, M., Whitmore, A. P., and Ritz, K.: Distinct respiratory responses of soils to complex organic substrate are governed predominantly by soil architecture and its microbial community, *Soil Biology and Biochemistry*, 103, 493–501, <https://doi.org/10.1016/j.soilbio.2016.09.015>, 2016.
- 15 Georgiou, K., Abramoff, R. Z., Harte, J., Riley, W. J., and Torn, M. S.: Microbial community-level regulation explains soil carbon responses to long-term litter manipulations, *Nature Communications*, 8, 1–10, <https://doi.org/10.1038/s41467-017-01116-z>, 2017.
- German, D. P., Marcelo, K. R. B., Stone, M. M., and Allison, S. D.: The Michaelis-Menten kinetics of soil extracellular enzymes in response to temperature: A cross-latitudinal study, *Global Change Biology*, 18, 1468–1479, <https://doi.org/10.1111/j.1365-2486.2011.02615.x>, 2012.
- 20 Ginovart, M. and Valls, J.: Individual Based Modelling of Microbial Activity to Study Mineralization and Nitrification Process in Soil, *AICME II abstracts*, 6, 1996, <https://doi.org/10.1016/j.nonrwa.2004.12.005>, 1996.
- Herbst, M., Tappe, W., Kummer, S., and Vereecken, H.: The impact of sieving on heterotrophic respiration response to water content in loamy and sandy topsoils, *Geoderma*, 272, 73–82, <https://doi.org/10.1016/j.geoderma.2016.03.002>, 2016.
- 25 Hunt, A. G. and Manzoni, S.: Networks on Networks, 2053-2571, Morgan & Claypool Publishers, <https://doi.org/10.1088/978-1-6817-4159-8>, 2015.
- Jenkinson, D. and Rayner, J.: The turnover of soil organic matter in some of the Rothamsted classical experiments, *Soil science*, 123, 298–305, 1977.
- 30 Jenny, H., Gessel, S., and Bingham, F.: Comparative study of decomposition rates of organic matter in temperate and tropical regions, *Soil Science*, 68, 419–432, 1949.

- Juarez, S., Nunan, N., Duday, A. C., Pouteau, V., Schmidt, S., Hapca, S., Falconer, R., Otten, W., and Chenu, C.: Effects of different soil structures on the decomposition of native and added organic carbon, *European Journal of Soil Biology*, 58, 81–90, <https://doi.org/10.1016/j.ejsobi.2013.06.005>, 2013.
- Kaiser, C., Franklin, O., Dieckmann, U., and Richter, A.: Microbial community dynamics alleviate stoichiometric constraints during litter decay, *Ecology Letters*, 17, 680–690, <https://doi.org/10.1111/ele.12269>, 2014.
- Keeling, M. J. J., Wilson, H. B. B., and Pacala, S. W. W.: Deterministic Limits to Stochastic Spatial Models of Natural Enemies, *The American naturalist*, 159, 57–80, <https://doi.org/10.1086/324119>, 2002.
- Killham, K., Amato, M., and Ladd, J. N.: Effect of substrate location in soil and soil pore-water regime on carbon turnover, *Soil Biology and Biochemistry*, 25, 57–62, [https://doi.org/10.1016/0038-0717\(93\)90241-3](https://doi.org/10.1016/0038-0717(93)90241-3), 1993.
- 10 Koestel, J. and Schlüter, S.: Quantification of the structure evolution in a garden soil over the course of two years, *Geoderma*, 338, 597 – 609, <https://doi.org/10.1016/j.geoderma.2018.12.030>, 2019.
- Kravchenko, A. N. and Guber, A. K.: Soil pores and their contributions to soil carbon processes, *Geoderma*, 287, 31–39, <https://doi.org/10.1016/j.geoderma.2016.06.027>, 2017.
- Kuzyakov, Y. and Blagodatskaya, E.: Microbial hotspots and hot moments in soil: concept & review, *Soil Biology and Biochemistry*, 83, 15 184–199, <https://doi.org/10.1016/j.soilbio.2015.01.025>, 2015.
- Lennon, J. J.: Red-shifts and red herrings in geographical ecology, *Ecography*, 23, 101–113, <https://doi.org/10.1111/j.1600-0587.2000.tb00265.x>, 2000.
- Lugo-Méndez, H. D., Valdés-Parada, F. J., Porter, M. L., Wood, B. D., and Ochoa-Tapia, J. A.: Upscaling Diffusion and Nonlinear Reactive Mass Transport in Homogeneous Porous Media, *Transport in Porous Media*, 107, 683–716, <https://doi.org/10.1007/s11242-015-0462-4>, 20 2015.
- Manzoni, S. and Katul, G.: Invariant soil water potential at zero microbial respiration explained by hydrological discontinuity in dry soils, *Geophysical Research Letters*, 41, 7151–7158, <https://doi.org/10.1002/2014GL061467>, 2014.
- Manzoni, S. and Porporato, A.: A theoretical analysis of nonlinearities and feedbacks in soil carbon and nitrogen cycles, *Soil Biology and Biochemistry*, 39, 1542–1556, <https://doi.org/10.1016/j.soilbio.2007.01.006>, 2007.
- 25 Manzoni, S. and Porporato, A.: Soil carbon and nitrogen mineralization: Theory and models across scales, *Soil Biology and Biochemistry*, 41, 1355–1379, <https://doi.org/10.1016/j.soilbio.2009.02.031>, 2009.
- Manzoni, S., Porporato, A., and Schimel, J. P.: Soil heterogeneity in lumped mineralization–immobilization models, *Soil Biology and Biochemistry*, 40, 1137–1148, <https://doi.org/10.1016/j.soilbio.2007.12.006>, 2008.
- Manzoni, S., Piñeiro, G., Jackson, R. B., Jobbágy, E. G., Kim, J. H., and Porporato, A.: Analytical models of soil and litter decomposition: Solutions for mass loss and time-dependent decay rates, *Soil Biology and Biochemistry*, 50, 66–76, 30 <https://doi.org/10.1016/j.soilbio.2012.02.029>, 2012.

- Melbourne, B. A. and Chesson, P.: The scale transition: Scaling up population dynamics with field data, *Ecology*, 87, 1478–1488, [https://doi.org/10.1890/0012-9658\(2006\)87\[1478:TSTSUP\]2.0.CO;2](https://doi.org/10.1890/0012-9658(2006)87[1478:TSTSUP]2.0.CO;2), 2006.
- Monga, O., Bousso, M., Garnier, P., and Pot, V.: 3D geometric structures and biological activity: Application to microbial soil organic matter decomposition in pore space, *Ecological Modelling*, 216, 291–302, <https://doi.org/10.1016/j.ecolmodel.2008.04.015>, 2008.
- 5 Monga, O., Garnier, P., Pot, V., Coucheney, E., Nunan, N., Otten, W., and Chenu, C.: Simulating microbial degradation of organic matter in a simple porous system using the 3-D diffusion-based model MOSAIC, *Biogeosciences*, 11, 2201–2209, <https://doi.org/10.5194/bg-11-2201-2014>, 2014.
- Morozov, A. and Poggiale, J. C.: From spatially explicit ecological models to mean-field dynamics: The state of the art and perspectives, *Ecological Complexity*, 10, 1–11, <https://doi.org/10.1016/j.ecocom.2012.04.001>, 2012.
- 10 Murrell, D. J., Dieckmann, U., and Law, R.: On moment closures for population dynamics in continuous space, *Journal of Theoretical Biology*, 229, 421–432, <https://doi.org/10.1016/j.jtbi.2004.04.013>, 2004.
- Negassa, W. C., Guber, A. K., Kravchenko, A. N., Marsh, T. L., Hildebrandt, B., and Rivers, M. L.: Properties of soil pore space regulate pathways of plant residue decomposition and community structure of associated bacteria, *PLoS ONE*, 10, 1–22, <https://doi.org/10.1371/journal.pone.0123999>, 2015.
- 15 Nguyen-Ngoc, D., Leye, B., Monga, O., Garnier, P., and Nunan, N.: Modeling Microbial Decomposition in Real 3D Soil Structures Using Partial Differential Equations, *International Journal of Geosciences*, 04, 15–26, <https://doi.org/10.4236/ijg.2013.410A003>, 2013.
- Nunan, N., Wu, K., Young, I. M., Crawford, J. W., and Ritz, K.: In situ spatial patterns of soil bacterial populations, mapped at multiple scales, in an arable soil, *Microbial Ecology*, 44, 296–305, <https://doi.org/10.1007/s00248-002-2021-0>, 2002.
- Nunan, N., Wu, K., Young, I. M., Crawford, J. W., and Ritz, K.: Spatial distribution of bacterial communities and their relationships with the micro-architecture of soil, *FEMS Microbiology Ecology*, 44, 203–215, [https://doi.org/10.1016/S0168-6496\(03\)00027-8](https://doi.org/10.1016/S0168-6496(03)00027-8), 2003.
- 20 Olson, J. S.: Energy Storage and the Balance of Producers and Decomposers in Ecological Systems, *Ecology*, 44, 322–331, <https://doi.org/10.2307/1932179>, 1963.
- Parton, W., Schimel, D. S., Cole, C., and Ojima, D.: Analysis of factors controlling soil organic matter levels in Great Plains Grasslands 1, *Soil Science Society of America Journal*, 51, 1173–1179, 1987.
- 25 Peth, S., Chenu, C., Leblond, N., Mordhorst, A., Garnier, P., Nunan, N., Pot, V., Ogurreck, M., and Beckmann, F.: Localization of soil organic matter in soil aggregates using synchrotron-based X-ray microtomography, *Soil Biology and Biochemistry*, 78, 189–194, <https://doi.org/10.1016/j.soilbio.2014.07.024>, 2014.
- Porter, M. L., Valdés-Parada, F. J., and Wood, B. D.: Multiscale modeling of chemotaxis in homogeneous porous media, *Water Resources Research*, 47, 1–13, <https://doi.org/10.1029/2010WR009646>, 2011.
- 30 Rawlins, B. G., Wragg, J., Reinhard, C., Atwood, R. C., Houston, A., Lark, R. M., and Rudolph, S.: Three-dimensional soil organic matter distribution, accessibility and microbial respiration in macroaggregates using osmium staining and synchrotron X-ray computed tomography, *Soil*, 2, 659–671, <https://doi.org/10.5194/soil-2-659-2016>, 2016.

- Raynaud, X. and Nunan, N.: Spatial ecology of bacteria at the microscale in soil, *PLoS ONE*, 9, <https://doi.org/10.1371/journal.pone.0087217>, 2014.
- Ruamps, L. S., Nunan, N., and Chenu, C.: Microbial biogeography at the soil pore scale, *Soil Biology and Biochemistry*, 43, 280–286, <https://doi.org/10.1016/J.SOILBIO.2010.10.010>, 2011.
- 5 Salomé, C., Nunan, N., Pouteau, V., Lerch, T. Z., and Chenu, C.: Carbon dynamics in topsoil and in subsoil may be controlled by different regulatory mechanisms, *Global Change Biology*, 16, 416–426, <https://doi.org/10.1111/j.1365-2486.2009.01884.x>, 2010.
- Schimel, J. P. and Weintraub, M. N.: The implications of exoenzyme activity on microbial carbon and nitrogen limitation in soil: A theoretical model, *Soil Biology and Biochemistry*, 35, 549–563, [https://doi.org/10.1016/S0038-0717\(03\)00015-4](https://doi.org/10.1016/S0038-0717(03)00015-4), 2003.
- Schmidt, M. W., Torn, M. S., Abiven, S., Dittmar, T., Guggenberger, G., Janssens, I. A., Kleber, M., Kögel-Knabner, I., Lehmann, J.,
10 Manning, D. A., Nannipieri, P., Rasse, D. P., Weiner, S., and Trumbore, S. E.: Persistence of soil organic matter as an ecosystem property, <https://doi.org/10.1038/nature10386>, 2011.
- Schnecker, J., Bowles, T., Hobbie, E. A., Smith, R. G., and Grandy, A. S.: Substrate quality and concentration control decomposition and microbial strategies in a model soil system, *Biogeochemistry*, pp. 1–13, 2019.
- Sierra, C. A. and Muller, M.: A general mathematical framework for representing soil organic matter dynamics, *Ecological Monographs*, 85,
15 505–524, <https://doi.org/10.1890/15-0361.1>, 2015.
- Stanley, C. E., Grossmann, G., i Solvas, X. C., and deMello, A. J.: Soil-on-a-Chip: Microfluidic Platforms for Environmental Organismal Studies, *Lab on a Chip*, 16, 228–241, <https://doi.org/10.1039/C5LC01285F>, 2016.
- Stenger, R., Barkle, G. F., and Burgess, C. P.: Mineralisation of organic matter in intact versus sieved/refilled soil cores, *Soil Research*, 40, 149–160, <https://doi.org/10.1071/SR01003>, 2002.
- 20 Tang, J. and Riley, W.: A total quasi-steady-state formulation of substrate uptake kinetics in complex networks and an example application to microbial litter decomposition, *Biogeosciences*, 10, 8329–8351, 2013.
- Tang, J.-Y. and Riley, W. J.: SUPECA kinetics for scaling redox reactions in networks of mixed substrates and consumers and an example application to aerobic soil respiration, 2017.
- Valdés-Parada, F. J., Porter, M. L., Narayanaswamy, K., Ford, R. M., and Wood, B. D.: Upscaling microbial chemotaxis in porous media,
25 *Advances in Water Resources*, 32, 1413–1428, <https://doi.org/10.1016/j.advwatres.2009.06.010>, 2009.
- Van Oijen, M., Cameron, D., Levy, P. E., and Preston, R.: Correcting errors from spatial upscaling of nonlinear greenhouse gas flux models, *Environmental Modelling & Software*, 94, 157–165, <https://doi.org/10.1016/j.envsoft.2017.03.023>, 2017.
- Wang, B. and Allison, S. D.: Emergent properties of organic matter decomposition by soil enzymes, *Soil Biology and Biochemistry*, p. 107522, 2019.
- 30 Watt, M., Silk, W. K., and Passioura, J. B.: Rates of root and organism growth, soil conditions, and temporal and spatial development of the rhizosphere, *Annals of botany*, 97, 839–855, <https://doi.org/10.1093/aob/mcl028>, 2006.

- Whitaker, S.: The Method of Volume Averaging, vol. 13 of *Theory and Applications of Transport in Porous Media*, Springer Netherlands, Dordrecht, <https://doi.org/10.1007/978-94-017-3389-2>, 1999.
- Wieder, W. R., Bonan, G. B., and Allison, S. D.: Global soil carbon projections are improved by modelling microbial processes, *Nature Climate Change*, 3, 909, <https://doi.org/10.1038/nclimate1951>, 2013.
- 5 Wieder, W. R., Allison, S. D., Davidson, E. A., Georgiou, K., Hararuk, O., He, Y., Hopkins, F., Luo, Y., Smith, M. J., Sulman, B., Todd-Brown, K., Wang, Y. P., Xia, J., and Xu, X.: Explicitly representing soil microbial processes in Earth system models, *Global Biogeochemical Cycles*, 29, 1782–1800, <https://doi.org/10.1002/2015GB005188>, 2015.
- Wieder, W. R., Hartman, M. D., Sulman, B. N., Wang, Y. P., Koven, C. D., and Bonan, G. B.: Carbon cycle confidence and uncertainty: Exploring variation among soil biogeochemical models, *Global Change Biology*, 24, 1563–1579, <https://doi.org/10.1111/gcb.13979>, 2018.
- 10 Witter, E.: Soil C balance in a long-term field experiment in relation to the size of the microbial biomass, *Biology and Fertility of Soils*, 23, 33–37, <https://doi.org/10.1007/BF00335815>, 1996.
- Wutzler, T. and Reichstein, M.: Colimitation of decomposition by substrate and decomposers — a comparison of model formulations, *Biogeosciences*, 5, 749–759, <https://doi.org/10.5194/bg-5-749-2008>, 2008.
- Xie, X. S.: Enzyme Kinetics, Past and Present, *Science*, 342, 1457–1459, <https://doi.org/10.1126/science.1248859>, 2013.
- 15 Xu, X., Thornton, P. E., and Post, W. M.: A global analysis of soil microbial biomass carbon, nitrogen and phosphorus in terrestrial ecosystems, *Global Ecology and Biogeography*, 22, 737–749, 2013.
- Yan, Z., Liu, C., Todd-Brown, K. E., Liu, Y., Bond-Lamberty, B., and Bailey, V. L.: Pore-scale investigation on the response of heterotrophic respiration to moisture conditions in heterogeneous soils, *Biogeochemistry*, 131, 121–134, <https://doi.org/10.1007/s10533-016-0270-0>, 2016.
- 20 Zelenev, V., Bruggen, A. V., and Semenov, A.: BACWAVE, a Spatial–Temporal Model for Traveling Waves of Bacterial Populations in Response to a Moving Carbon Source in Soil, *Microbial ecology*, 40, 260–272, <https://doi.org/10.1007/s002480000029>, 2000.